ANALYSIS OF PRESSURE WAVE PROPAGATION IN MULTIPHASE FLOW IN OIL PRODUCTION LINES AND NUMERICAL MODELING OF PROCESS

A THESIS SUBMITTED TO
THE GRADUATE SCHOOL OF NATURAL AND APPLIED SCIENCES
OF
MIDDLE EAST TECHNICAL UNIVERSITY

BY

RABİA TUĞÇE ÖZDEMİR

IN PARTIAL FULFILLMENT OF THE REQUIREMENTS
FOR
THE DEGREE OF DOCTOR OF PHILOSOPHY
IN
PETROLEUM AND NATURAL GAS ENGINEERING

JULY 2024

Approval of the thesis:

ANALYSIS OF PRESSURE WAVE PROPAGATION IN MULTIPHASE FLOW IN OIL PRODUCTION LINES AND NUMERICAL MODELING OF PROCESS

submitted by **RABİA TUĞÇE ÖZDEMİR** in partial fulfillment of the requirements for the degree of **Doctor of Philosophy** i**n Petroleum and Natural Gas Engineering, Middle East Technical University** by,

Prof. Dr. Naci Emre Altun
Dean, **Graduate School of Natural and Applied Sciences** _____

Assoc. Prof. Dr. İsmail Durgut
Head of Department, **Petroleum and Natural Gas Engineering** _____

Assoc. Prof. Dr. İsmail Durgut
Supervisor, **Petroleum and Natural Gas Engineering Dept., METU** _____

Examining Committee Members:

Prof. Dr. Mahmut Parlaktuna
Petroleum and Natural Gas Eng, METU _____

Assoc. Prof. Dr. İsmail Durgut
Petroleum and Natural Gas Eng, METU _____

Assoc. Prof. Dr. Çağlar Sinayuc
Petroleum and Natural Gas Eng, METU _____

Prof. Dr. Ömer İnanç Türeyen
Petroleum and Natural Gas Eng, İTÜ _____

Assoc. Prof. Dr. Fazıl Emre Artun
Petroleum and Natural Gas Eng., Sultan Qaboos University _____

Date: 25.07.2024

I hereby declare that all information in this document has been obtained and presented in accordance with academic rules and ethical conduct. I also declare that, as required by these rules and conduct, I have fully cited and referenced all material and results that are not original to this work.

Name Last name: Rabia Tuğçe Özdemir

Signature:

ABSTRACT

ANALYSIS OF PRESSURE WAVE PROPAGATION IN MULTIPHASE FLOW IN OIL PRODUCTION LINES AND NUMERICAL MODELING OF PROCESS

Özdemir, Rabia Tuğçe
Doctor of Philosophy, Petroleum and Natural Gas Engineering
Supervisor: Assoc. Prof. Dr. İsmail Durgut

July 2024, 97 pages

Pressure propagation in pipelines plays a critical role in analyzing fluid flow behavior and optimizing the transportation of multiphase flows in various industries, including the oil and gas sector. Understanding this process in these multiphase flows offers valuable insights into their composition, phase distribution, and flow regime, enabling efficient and safe pipeline operations. This study offers a comprehensive examination of pressure propagation in pipelines, a particularly significant phenomenon in the transportation of multiphase flows within the oil and gas industry.

The core of this research lies in a method developed to determine the speed of pressure waves in multiphase fluid flows along oil production lines. Data were collected during a testing operation conducted on an offshore production platform in the North Sea. The method emerged from detailed observations of pressure propagations along production lines during normal operational activities. Pressure signals, potentially generated by such activities or by the transient dynamics inherent to multiphase flow, were recorded at two distinct locations along the production line. These signals were then subjected to cross-correlation analysis to calculate the flight time of the signal, thereby determining the speed of the pressure waves.

The measured speed of pressure waves in the multiphase fluid was compared against two established empirical models—the Wood model and the Dong and Gudmundsson model—both of which calculate the speed of sound based on fluid properties, gas-oil ratio (GOR), water cut, pressure, and temperature. Additionally, the measurements were compared with simulation results from a transient multiphase flow simulator, utilizing the same PVT properties. The analysis revealed that the Wood model tends to overestimate the speed of sound, particularly at higher pressures. In contrast, the Dong and Gudmundsson model offers closer approximations to the measured pressure wave propagation speed. Moreover, the transient flow simulator strongly correlated with the measured data across almost the entire pressure range, reinforcing its reliability.

In addition to the empirical measurements and comparisons with established models, this study also incorporates numerical modeling to further investigate the effects of pressure wave propagation in pipelines. Both 1-D and 2-D numerical models were employed to analyze how pressure waves behave within the pipeline system. The results from these models revealed that the speed of sound significantly impacts the amplitude of a pressure pulse, particularly when the velocity changes gradually or when the pulse encounters a discontinuity. Specifically, when a pressure pulse moves from a low-speed region to a high-speed region, it results in a transmitted pulse with higher pressure.

While these effects were detectable in the 2-D model, the complexity of the model posed challenges in calculating the propagation speed of pressure waves as effectively as in the 1-D model. The 1-D model, with its simplified assumptions, allowed for a more straightforward calculation of wave propagation speed, whereas the 2-D model's complexity necessitated a more detailed analysis.

Keywords: Multiphase flow, Pressure wave propagation, Cross-correlation

ÖZ

PETROL ÜRETİM HATLARINDA ÇOK FAZLI AKIŞTA BASINÇ DALGASI YAYILIMININ ANALİZİ VE SÜRECİN SAYISAL MODELLEMESİ

Özdemir, Rabia Tuğçe
Doktora, Petrol ve Doğal gaz Mühendisliği
Tez Yöneticisi: Doç. İsmail Durgut

Temmuz 2024, 97 sayfa

Boru hatlarındaki basınç yayılımı, çok fazlı akışların çeşitli endüstrilerde, özellikle petrol ve gaz sektöründe taşınmasının analizinde ve optimizasyonunda kritik bir rol oynar. Bu süreç hakkında bilgi sahibi olmak, bu çok fazlı akışların bileşimi, faz dağılımı ve akış rejimi hakkında değerli bilgiler sunar ve boru hattı operasyonlarının verimli ve güvenli bir şekilde yönetilmesini sağlar. Bu çalışma, çok fazlı akışların taşınması sırasında özellikle önemli bir fenomen olan boru hatlarındaki basınç yayılımının kapsamlı bir incelemesini sunmaktadır.

Araştırmanın merkezi, çok fazlı sıvı akışlarındaki basınç dalgalarının hızını belirlemek için geliştirilmiş bir yöntemdir. Veriler, Kuzey Denizi'nde bir deniz üretim platformunda gerçekleştirilen bir test operasyonu sırasında toplanmıştır. Yöntem, üretim hatlarındaki normal operasyonel faaliyetler sırasında basınç yayılımlarının detaylı gözlemlerinden doğmuştur. Bu tür faaliyetlerden veya çok fazlı akışın geçici dinamiklerinden kaynaklanan basınç sinyalleri, üretim hattının iki farklı noktasında kaydedilmiştir. Bu sinyaller, sinyalin uçuş süresini hesaplamak ve böylece basınç dalgalarının hızını belirlemek için çapraz korelasyon analizine tabi tutulmuştur.

Çok fazlı sıvıdaki basınç dalgalarının ölçülen hızı, sıvı özelliklerine, gaz-petrol oranına (GOR), su kesiti, basınç ve sıcaklığa dayalı olarak ses hızını hesaplayan iki yerleşik ampirik model—Wood modeli ve Dong ve Gudmundsson modeli—ile karşılaştırılmıştır. Ayrıca, aynı PVT özelliklerini kullanarak yapılan bir geçici çok fazlı akış simülatöründen elde edilen simülasyon sonuçları ile de karşılaştırılmıştır. Analiz, Wood modelinin özellikle yüksek basınçlarda ses hızını fazla tahmin etme eğiliminde olduğunu ortaya koymuştur. Buna karşılık, Dong ve Gudmundsson modeli, ölçülen basınç dalgası yayılım hızına daha yakın tahminler sunmaktadır. Ayrıca, geçici akış simülatörü, ölçülen verilerle neredeyse tüm basınç aralığında güçlü bir korelasyon göstererek güvenilirliğini pekiştirmiştir.

Bu ampirik ölçümler ve yerleşik modellerle yapılan karşılaştırmaların yanı sıra, bu çalışma, boru hatlarındaki basınç dalgası yayılımının etkilerini daha fazla araştırmak için sayısal modellemeyi de içermektedir. Basınç dalgalarının boru hattı sistemi içinde nasıl davrandığını analiz etmek için hem 1-D hem de 2-D sayısal modeller kullanılmıştır. Bu modellerin sonuçları, ses hızının basınç dalgasının genliğini önemli ölçüde etkilediğini, özellikle hızın yavaşça değiştiği durumlarda veya dalga bir kesintiye uğradığında ortaya koymuştur. Özellikle, bir basınç dalgası düşük hız bölgesinden yüksek hız bölgesine geçtiğinde, daha yüksek basınçlı bir iletilen dalga meydana gelir.

Bu etkiler 2-D modelde tespit edilebilse de, modelin karmaşıklığı, basınç dalgalarının yayılma hızını 1-D modelde olduğu kadar etkili bir şekilde hesaplamada zorluklar yaratmıştır. 1-D model, basitleştirilmiş varsayımlarıyla dalga yayılma hızının daha kolay hesaplanmasına olanak tanırken, 2-D modelin karmaşıklığı daha ayrıntılı bir analizi zorunlu kılmıştır.

Anahtar Kelimeler: Çoklu akış, Basınç dalgalarının yayılması, Çapraz korelasyon

To My Beloved Family

ACKNOWLEDGMENTS

First and foremost, I would like to express my deepest gratitude to my supervisor, Assoc. Prof. Dr. İsmail Durgut, for his invaluable guidance, unwavering support, inspiration and constant encouragement throughout the course of my research. His wisdom and experience have greatly enriched my work, and I am truly thankful for his contributions. Special thanks go to Assoc. Prof Dr. Çağlar Sınayuç and Assoc. Prof Dr. Emre Artun as my PhD thesis committee members. Their technical expertise, collaborative spirit, and continuous support have been essential in the completion of this research. I deeply appreciate their contributions and companionship. I am also profoundly grateful to Prof. Dr. Mahmut Parlaktuna for his expert advice, constructive criticism, and generous assistance. I would also like to extend my heartfelt thanks to my friends Betül Yıldırım, İnanç Alptuğ Hıdıroğlu and Onur Alp Kaya. Their friendship, encouragement, and belief in me have provided the emotional support I needed during the challenging times of my PhD journey. Last but certainly not least, I would like to extend my heartfelt thanks to my dear family. Their unconditional love, patience, and support have been my foundation and source of strength throughout this journey. Without them, this achievement would not have been possible. Thank you all for being part of this incredible journey.

TABLE OF CONTENTS

LIST OF TABLES

LIST OF FIGURES

NOMENCLATURE

α void fraction (-)

β water-oil volumetric fraction (-)

γ ratio of specific heats (-)

δ_{ij} Kronecker delta

ξ_1, ξ_2 computational domain dimensions

μ dynamic viscosity of the fluid (cp)

λ eigenvalue

ρ density (kg/m^3)

τ time delay (s)

A total area of pipe

A_G area occupied by gas phase (m^2)

B_g gas formation volume factor (m^3/Sm^3)

B_o oil formation volume factor (m^3/Sm^3)

B_w water formation volume factor (m^3/Sm^3)

c speed of sound (m/s)

C_P isotropic specific heat capacity (J/K-mol)

C_V volumetric specific heat capacity (J/K-mol)

C_{ij} regions occupied by the grid cell in physical domain

$D = D(x)$ flow diameter (m)

e internal energy (J)

E total energy (J)

f friction coefficient (-)

g acceleration of gravity (m/s^2)

GOR gas oil ratio (-)

H_L liquid holdup (-)

$J(C_{ij})$ Jacobian of the mapping of the cell

K^T isothermal compressibility (1/Pa)

K^S isentropic compressibility (1/Pa)

$M(C_{ij})$ measure area of C_{ij}

N_d number of spatial dimensions

P pressure (bara, Pa)

Q_G flow rate of gas phase (m^3/d)

Q_L flow rate of liquid phase (m^3/d)

r eigenvector

$R(\tau)$ cross correlation function

u_j velocity in x_j direction (m/s)

v cross-sectional average fluid flow velocity (m/s)

V total volume (m^3)

V_L volume occupied by liquid phase (m^3)

V_M mixture velocity (m^2/s)

V_{SG} superficial velocity of gas phase (m^2/s)

V_{SL} superficial velocity of liquid phase (m^2/s)

V_{Slip} slip velocity (m^2/s)

WC water cut ()

x gas-liquid mass fraction (-)

y water-liquid mass fraction (-)

z opposite direction of gravity (m/s^2)

subscript G *and* L *represent gas and liquid phases, respectively*

superscript + *and* – *represent right and left going fluctuations, respectively*

CHAPTER 1

INTRODUCTION

Multiphase flow is a fundamental and complex phenomenon crucial in various industries, particularly in the oil and gas sector. In the context of pipelines, multiphase flow refers to the simultaneous transportation of multiple phases within the same conduit, such as gas, oil, water, and solids. This complex transport of heterogeneous mixtures presents a significant challenge in the industry, as it directly influences the overall efficiency, safety, and cost-effectiveness of hydrocarbon production and transportation processes.(Al-Safran & Brill, 2017, Gudmundsson, 1998). As a result, the effective metering and monitoring of multiphase flow are critical for optimizing oilfield operations and ensuring the sustainable and reliable extraction and transportation of hydrocarbons. (Williams, 1994, Retnanto & Azim, 2001, Al-Kadem et al., 2014, Graham et al., 2022).

However, various factors, including the lack of affordable and proven technology, have hindered the widespread adoption of multiphase metering in the petroleum industry. Accurate prediction, monitoring, and control of multiphase flow in pipelines require sophisticated measurement techniques and instruments that can withstand harsh operating conditions (Al-Kadem et al., 2022). Therefore, developing cost-effective, reliable, and accurate multiphase flow metering technologies has become a focal point of research and innovation within the oil and gas industry.

Efficient oil and gas transportation through pipelines is crucial for the energy industry. Pressure wave propagation in multiphase flow, influenced by factors such as leaks, viscosity changes, and flow regime transitions, is a critical aspect of pipeline performance (Guo et al., 2022; Li et al., 2023). This study aims to provide

an in-depth numerical and signal processing investigation of pressure wave propagation in multiphase flow within oil production lines.

The presence of leaks in oil pipelines can have significant consequences, including environmental damage and economic losses. (Li et al., 2023). Real-time transient models can calculate various fluid properties, such as flow, pressure, temperature, and density, along the pipeline, allowing operators to make informed decisions and respond quickly to incidents. Simulation-based studies have been conducted to evaluate the thermo-fluid dynamics of transient three-phase flow in the presence of leaks, providing insights into the velocity, pressure, and volume fraction fields of the involved phases.

The current work aims to build on these previous studies by conducting a comprehensive numerical and signal processing investigation of pressure wave propagation in multiphase flow within oil production lines. The research will focus on developing advanced models that can accurately capture the complex phenomena associated with pressure wave propagation, including the effects of leaks, viscosity changes, and flow regime transitions.

The field-scale approach employed in this study proposes a novel method for calculating the speed of pressure waves based on pressure signals from two transmitters. Data was collected during a testing campaign conducted on an offshore production platform in the North Sea. The method has been based and emerged on observations of pressure propagations along production lines during normal operational activities. Pressure signals that might have been generated due to such activities or the transient dynamics of multiphase flow were recorded at two different locations along the production line. These signals were then cross-correlated, and the flight time of the signal was calculated. The measured pressure wave propagation speed values in the multiphase fluid are compared with two different empirical models, which compute the speed of sound from fluid properties, GOR, water cut and pressure, and temperature. In addition, by using the

same PVT properties, the measurements are compared with the simulation results from a transient multiphase flow simulator. The chosen technique involves utilizing the cross-correlation method, which effectively extracts relevant information from the transmitted signals. We aim to derive accurate and meaningful propagation speed of pressure waves data by applying this method to the pressure signals. This streamlined approach facilitates computational efficiency and offers a practical and reliable means to assess the acoustic behaviour within the system.

In addition, our study is aimed at presenting 1-D and 2-D numerical models for the propagation of pressure waves in pipelines. The results of our investigation will be rigorously compared using both established field scale and numerical methods. This comparative analysis will provide a comprehensive conclusion, shedding light on the accuracy and applicability of our modeled the speed of pressure waves across a range of void fractions. Through this research, we intend to contribute valuable insights into understanding acoustic behavior in different flow regimes and to provide a basis for further advancements in fluid dynamics modeling.

CHAPTER 2

LITERATURE REVIEW

The flow of multiphase fluids through pipelines is a critical aspect of various industries, including oil and gas, where the simultaneous presence of gas, liquid, and solid phases poses unique challenges. Understanding the dynamics of multiphase flow in pipelines and the associated pressure propagation phenomena is imperative for ensuring these systems' safe and efficient operation. This chapter provides a comprehensive literature review of the current state of knowledge. It explores fundamental theories contributing to our understanding of multiphase flow behavior and pressure dynamics in pipelines.

2.1 Multiphase Flow in Pipelines

Multiphase flow is a fundamental and complex phenomenon crucial in various industries, particularly in the oil and gas sector. In the context of pipelines, multiphase flow refers to the simultaneous transportation of multiple phases within the same conduit, such as gas, oil, water, and solids. This complex transport of heterogeneous mixtures presents a significant challenge in the industry, as it directly influences the overall efficiency, safety, and cost-effectiveness of hydrocarbon production and transportation processes. As a result, the effective metering and monitoring of multiphase flow are critical for optimizing oilfield operations and ensuring the sustainable and reliable extraction and transportation of hydrocarbons.

The study of multiphase flow is crucial in various fields, including engineering, physics, and environmental science, as many natural and industrial processes involve the interaction of different phases.

The phases involved in multiphase flow are typically categorised as follows:

- **Gas-liquid flow** is one of the most common types of multiphase flow, where a gas phase (such as air or vapor) coexists with a liquid phase (such as water or oil). Examples include natural gas and oil flow in pipelines, bubble columns, and air-water flow in pipes.
- **Liquid-Liquid Flow:** In this case, two immiscible liquid phases flow together. An example is the transport of oil and water in pipelines.
- **Gas-Solid Flow:** This involves the movement of a gas phase carrying solid particles. Examples include pneumatic conveying systems and fluidized bed reactors.
- **Gas-Liquid-Solid Flow:** This type includes all three phases interacting simultaneously. An example is oil, gas, and sand transport in oil and gas production processes.

Understanding multiphase flow is crucial because it affects the performance and efficiency of many industrial processes. For example:

- **Oil and Gas Industry:** Multiphase flow is encountered in oil and gas transportation through pipelines. Understanding how different phases behave is essential to optimizing pipeline design and operation.
- **Chemical Engineering:** Multiphase reactors are used in various chemical processes. Knowledge of multiphase flow is essential for designing and optimizing these reactors.
- **Environmental Engineering:** Understanding multiphase flow is essential in modeling natural processes such as sediment transport in rivers and coastal areas.

Researchers and engineers use various experimental and computational techniques to study multiphase flow, including flow visualization, numerical simulations, and

laboratory experiments. The complexity of multiphase flow makes it a challenging but fascinating study area with wide-ranging applications.

2.1.1 Flow Regimes

Multiphase flow in pipelines can exhibit various flow regimes, which are distinct patterns of flow behavior. The description of flow patterns tends to be more qualitative than quantitative. The observed flow patterns are ascribed to different variables by different researchers. (Barbosa et al., 2010; Barnea et al., 1980; Crawford et al., 1985; Rosa et al., 2012; Wallis, 1969).

A flow regime refers to the distinct patterns and behaviors exhibited by different phases as they move through a pipeline. Factors such as flow rates, fluid properties, and pipeline geometry influence the transitions between these regimes. Common flow regimes include slug flow, stratified flow, annular flow, and plug flow, each presenting unique challenges and opportunities for system engineers and operators.

2.1.1.1 Flow Patterns in Vertical Pipelines

The flow regime in vertical pipelines refers to the distinct patterns of gas-liquid interaction that occur as the two phases move upward within the conduit. Specific behaviors, distribution patterns, and physical phenomena characterize these flow regimes. As gas and liquid phases ascend in a vertical pipeline, their interactions give rise to different flow regimes, each with its own set of characteristics (Figure 2.1).

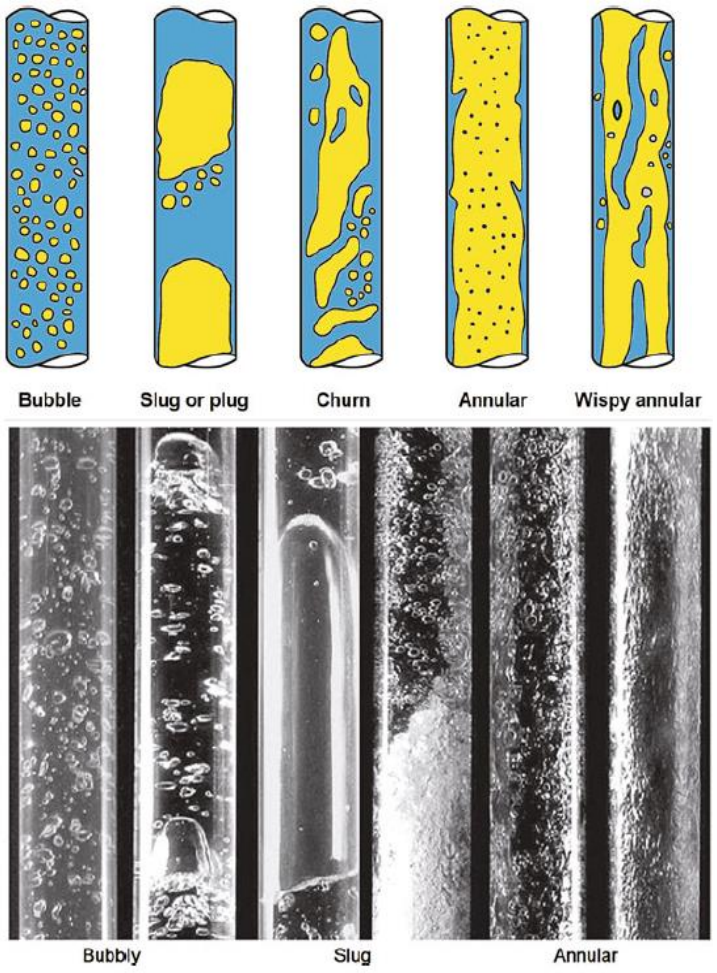

Figure 2.1. Sketches and photographs for flow patterns in vertical pipelines (Rosa et al., 2012)

Common flow regimes in vertical pipelines include:

- **Bubble flow:** In vertical pipes, the bubble flow phenomenon entails the intermittent rise of small gas bubbles within a liquid phase during their journey upwards in the conduit. These gas bubbles are dispersed throughout the liquid, varying in size and spacing, creating a dynamic visual display. As opposed to continuous liquid film regimes, the bubble flow pattern features a distinct boundary between the gas bubbles and the surrounding liquid, giving it a visually striking and easily identifiable appearance.

- **Slug flow:** Flow of slug in a vertical pipe is known for the periodic appearance of large bullet-shaped gas bubbles referred to as Taylor bubbles. As the gas flow rate increases, the closeness between bubbles becomes stronger, resulting in collisions and merging. Taylor bubbles can take up a considerable part of the pipe, bridging it, with diameters almost matching the pipe diameter. The area between Taylor bubbles and the pipe wall is filled with a downward-flowing liquid film. Sequential Taylor bubbles are divided by slugs of continuous liquid containing small gas bubbles. In vertical pipes, slug flow displays symmetry around the pipe axis. Some scholars differentiate between plug flow and slug flow. They define plug flow as occurring at slower gas flow rates with well-defined boundaries and bubble-free liquid slugs. Slug flow, on the other hand, occurs at faster gas flow rates, having less distinct boundaries and creating froth—a mass of small bubbles in the liquid. (Noble, 2018).
- **Churn flow:** The behavior of vertical pipe flow can include a phenomenon known as churn flow, which is defined as a turbulent two-phase flow regime characterized by the continuous intermingling of gas and liquid phases. Unlike other flow regimes, churn flow is distinguished by the absence of distinct boundaries between the gas and liquid phases. Instead, it comprises a highly turbulent and intermixed mixture of both phases. This complicated interaction between the gas and liquid results in a chaotic motion within the pipe as the churning of a turbulent fluid. Notably, churn flow in vertical pipes lacks a distinct interface between the gas and liquid phases, leading to a bubbly and turbulent mixture with dispersed gas bubbles throughout the liquid phase. The persistent churning motion of the mixture distinguishes churn flow from other flow patterns and is frequently observed at higher gas flow rates in vertical pipes, where the strong interaction between gas and liquid inhibits the formation of well-defined boundaries.

- **Annular flow:** In this scenario, most of the liquid flows along the wall of the duct in a thin film, while the gas occupies the central space as a continuous phase. It's common for some liquid to be carried within the gas core in the form of droplets, and vice versa, with some gas present in the liquid film as bubbles. When the gas velocity is high enough, large waves can form at the boundary between the liquid and gas. These waves can break apart, leading to the continuous addition of droplets to the gas core. It is worth noting that the reason why the liquid adheres to the wall and creates annular flow is not easily explained and likely involves intricate fluid dynamics and interfacial processes. Additionally, droplets from the gas core may settle on the liquid film, a phenomenon known as deposition or redeposition. Understanding annular flow requires considering the complex interactions between gas and liquid phases, wave dynamics, and entrainment mechanisms.

2.1.1.2 Flow Patterns in Horizontal Pipelines

The fluid flow dynamics in horizontal pipelines distinguish themselves from vertical flows, primarily due to the gravitational effects that induce stratification in the flow. In bubble and plug flow patterns, the upward movement of gas bubbles is notable. In stratified flow, the gas phase and liquid interaction generate surface waves (stratified-wavy flow) that may grow into large forms, transitioning into semi-slug flow. In some instances, these waves can reach the top of the tube, leading to slug flow. Horizontal tubes can also exhibit annular-dispersed flow, typically characterized by significant differences in film thickness between the lower and upper sections of the tube. It is practical to collectively categorize elongated bubble, plug, semi-slug, and slug flows as intermittent flows (Wallis, 1969; Yadigaroglu et al., 2018) (Figure 2.2).

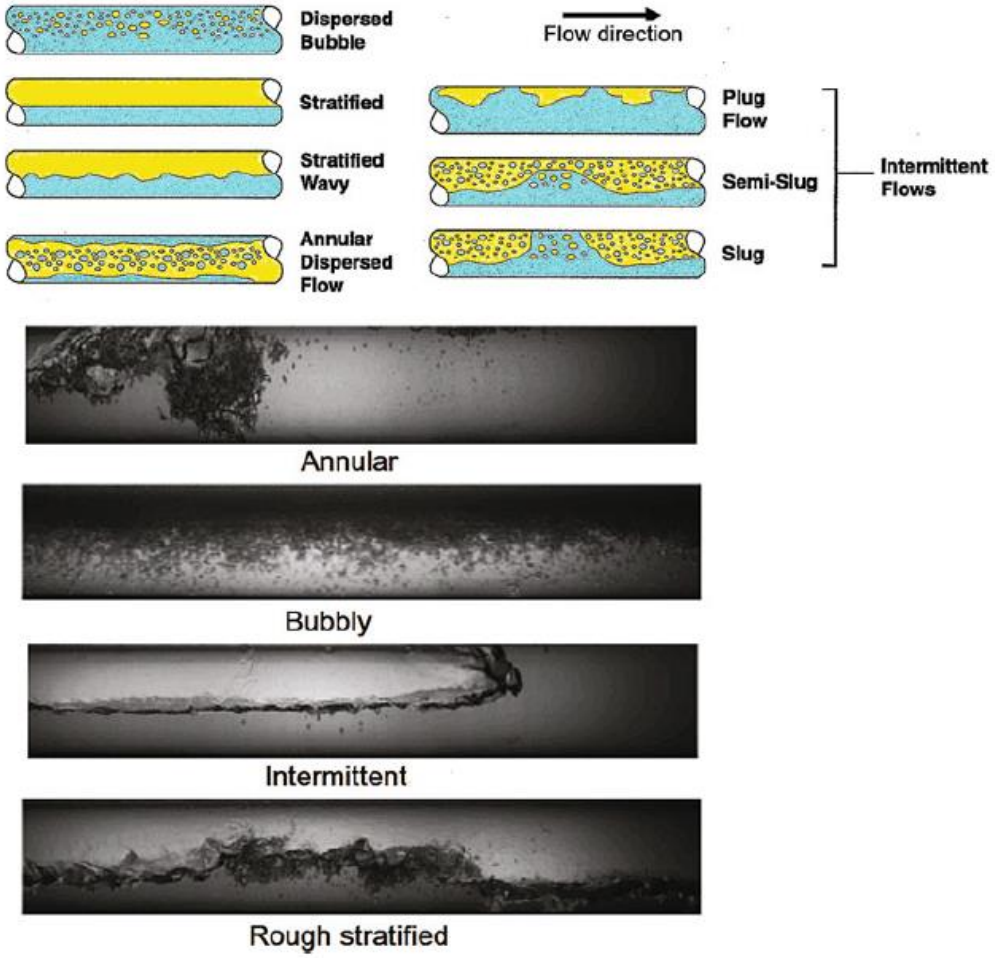

Figure 2.2. Sketches and photographs of flow patterns in horizontal pipes (Barbosa et al., 2010)

- **Bubble flow:** The continuous liquid in the tube contains dispersed bubbles, and their concentrations typically show a higher tendency in the upper section. With increased velocity, where the impact of gravity is diminished, the bubbles tend to achieve a more uniform dispersion throughout the tube.
- **Stratified flow:** Under typical gravitational conditions, the two phases in the tube are distinctly separated, with the liquid primarily situated at the bottom. This flow configuration is prevalent at low velocities for both liquid and gas and can exhibit either a smooth or wavy stratified pattern. The smooth stratified pattern is observed at lower gas velocities. As the gas

velocity increases, waves develop along the liquid-gas interface, progressing in the flow direction. The amplitude of these waves is influenced by the relative velocity between the phases and the inherent properties of the fluids, such as their densities and surface tension. This flow phenomenon is particularly pronounced under conditions of modest liquid and gas velocities.

- **Annular flow:** Increased gas flow rates induce the development of a liquid film on the tube wall, reminiscent of what is observed in vertical flow. An important deviation, however, is that the film at the bottom of the tube may have a considerably greater thickness compared to the film at the top, a variance influenced by the gas velocity and the relative impact of gravity. The continuity of the film around the tube's periphery may vary. The film might exhibit wavy patterns, akin to vertical flow, and commonly involves the dispersion of droplets within the gas core.
- **Plug/Slug flow:** Plug flow in horizontal pipes, also known as elongated bubble flow, is characterized by intermittent fluid motion, particularly observed at low flow rates and moderate liquid rates. In this regime, distinct liquid plugs, devoid of entrained gas bubbles, alternate with zones featuring elongated gas bubbles. The pattern manifests as well-defined slugs of liquid separated by regions of gas, contributing to the plug-like structure of the flow. The significance of gravity influences the downward motion of liquid slugs. This flow regime is particularly relevant at lower flow rates and offers a segmented structure where liquid plugs are distinct from the elongated gas bubble zones.

The studies Lee (1993) and Neogi et al. (1994) both highlight the significant impact of liquid compositions on flow regime transitions in oil-water-gas mixtures in horizontal pipelines. Lee's work specifically emphasizes the differences in flow regime transitions for these mixtures compared to gas-liquid and oil-water systems. Neogi's model further supports this, providing a

predictive tool for oil and water film thicknesses in three-phase stratified flow. Wang et al. (2016) builds on this by introducing experimental tomographic methods for analyzing the flow dynamics of gas-oil-water flows in horizontal pipelines, providing a valuable tool for visualizing these complex multiphase flows.

2.2 General Concepts of Multiphase Flow

Accurately determining the flow characteristics of fluid mixtures and the specific properties of individual phases or components is essential for a dependable analysis of two-phase flow. When two different fluids combine, it's crucial to find a method for describing the resulting mixture. This begins with estimating the probable properties and flow characteristics of the new mixture. The decision of whether to characterize the properties and overall variables of the mixture as averages or as a summation of the individual properties and variables of each phase or component is the focus of the study of two-phase flow properties and variables. Following discussion explores some key aspects of these properties and variables in two-phase flow.

2.2.1 Superficial Velocity

In multiphase flow, superficial velocity refers to the apparent velocity of one phase (either gas or liquid) as if that phase were the only one flowing in the conduit. It is a measure of the flow rate per unit cross-sectional area and is expressed in units of velocity (e.g., meters per second or feet per second).

Mathematically, the superficial velocity (V_S) for a particular phase is calculated by dividing the volumetric flow rate (Q) of that phase by the cross-sectional area (A) through which it is flowing for liquid phase:

$$V_{SL} = \frac{Q_L}{A} \tag{2.1}$$

and for gas phase:

$$V_{SG} = \frac{Q_G}{A} \tag{2.2}$$

The mixture velocity, V_M is estimated by:

$$V_M = V_{SL} + V_{SG} \tag{2.3}$$

Superficial velocity is a useful parameter in the analysis of two-phase flow systems because it provides an indication of the flow rate of each phase without considering their individual volume fractions. This parameter is essential for understanding the flow patterns, pressure drops, and overall behavior of gas-liquid systems

2.2.2 Slip Velocity

The term "slip velocity" or "velocity ratio" refers to the relative motion between different phases within a fluid mixture. A slip condition occurs when these phases exhibit varying velocities, commonly referred to as phase velocities. In the context of two-phase flow, slip is defined as the difference between the superficial velocities of the gas and liquid phases. In essence, it represents the difference between their true velocities in a given flow scenario. Mathematically the slip velocity is calculated by:

$$V_{slip} = V_{SG} - V_{SL} \tag{2.4}$$

2.3 Flow Pattern Maps

Flow pattern maps are indispensable tools in the field of multiphase flow research and engineering, providing a visual representation of the complex dynamics that occur within pipelines. In the realm of fluid mechanics, especially in scenarios involving the simultaneous movement of gas and liquid phases, understanding the prevailing flow patterns is crucial for optimizing system performance, ensuring safety, and minimizing operational risks.

Flow pattern maps serve as valuable guide for engineers and researchers, aiding in the selection of appropriate models, designing efficient separation devices, and predicting potential flow instabilities. By providing a visual roadmap of multiphase flow behavior, these maps contribute significantly to the development of strategies for optimizing the performance of oil and gas production systems, as well as various other industrial processes involving complex fluid dynamics. As research in a multiphase flow continues to evolve, flow pattern maps remain an essential tool for unraveling the intricacies of fluid behavior in pipelines and guiding advancements in engineering practices.

For air/ water and water/steam systems Hewitt & Roberts's (1969) map is appropriate in a range of pressure in considerably small diameter pipes. This map is constructed on the superficial velocities and density of the gas and liquid phases as its axes to delineate regions corresponding to various flow patterns.

Taitel & Dukler (1976) created a widely recognized flow regime map for horizontal two-phase flow according to superficial velocities of gas and liquid phase (Figure 2.3). As highlighted by Guo et al., (2014) this map was based on mechanistic models and has become a key tool in understanding and predicting flow behaviors in various engineering applications. The transitions between different flow regimes on the map are determined by several parameters including pressure gradient for single-phase gas and liquid flow, pipeline inclination angle, and liquid kinematic viscosity.

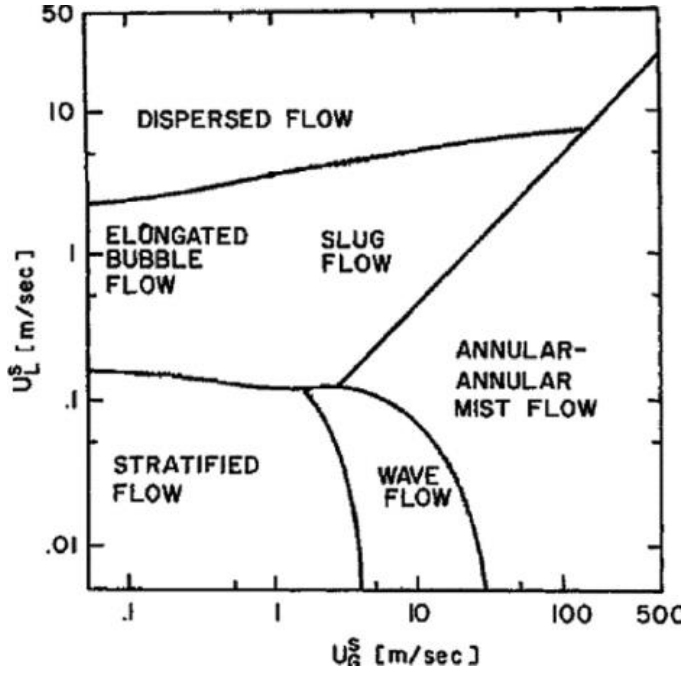

Figure 2.3. Taitel and Dukler's map for horizontal tubes (Taitel Y. & Dukler A. E., 1976)

Moreover, Mandhane et al., (1974) flow pattern map is another important tool used to classify and predict the flow regimes in horizontal two-phase flow, specifically for gas-liquid mixtures in pipes. It is similar in function to the Hewitt and Roberts map but is presented in a different format and is widely used in the industry for its practical application.

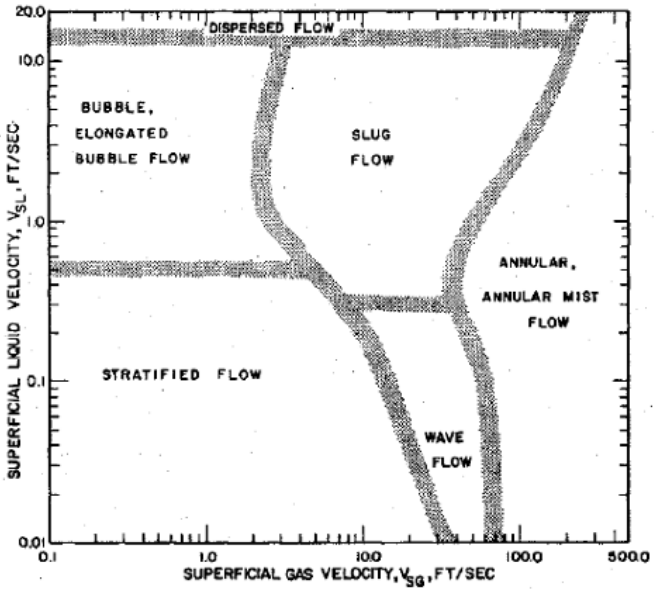

Figure 2.4. Mandanhe, Gregory, and Aziz map (Mandhane et al., 1974)

2.4 Multiphase Flow Models

Multiphase flow modeling is a crucial aspect of various engineering disciplines, encompassing chemical, petroleum, and environmental engineering fields. These models aim to capture the complex interactions between multiple phases within a given system, often involving fluids, solids, and gases.

In the study of multiphase flow, two primary types of models are frequently used: empirical models and mechanistic models. Each type has its strengths and limitations, and they are often employed in a complementary manner to enhance the understanding and prediction of multiphase flow behaviors.

Empirical models are based on experimental data and are typically focused on steady-state conditions. These models rely on empirical correlations to estimate various parameters, which are crucial when there is an incomplete physical understanding of the underlying phenomena involved in multiphase flows (Barnea et al., 1980, Beggs & Brill, 1973, Brustur, 2014).. By incorporating empirical

correlations into mechanistic models, researchers can optimize and simplify these models, leading to more accurate predictions and improved performance.

Empirical models enhance the accuracy of mechanistic models in multiphase flow studies. By leveraging a data-driven approach, the selection of the most accurate model can be based on the fit of various empirical correlations to the experimental data. This methodology ultimately improves the overall modeling capability in multiphase flow scenarios (Kozubkova et al., 2019; Usov et al., 2020).

For instance, the Lockhart-Martinelli correlation Lockhart (1949) provides a means to predict pressure drop in two-phase flows, and the Beggs and Brill correlation (Beggs & Brill, 1973) addresses the flow of gas-liquid mixtures in inclined pipes. The Hagedorn and Brown correlation (Hagedorn & Brown, 1965) is another significant empirical model, focusing on pressure gradients in vertical conduits. Additionally, Chisholm's work (Chisholm, 1967) offers theoretical backing for the Lockhart-Martinelli correlation, enhancing its applicability.

Mechanistic models are grounded in the fundamental principles of physics and attempt to describe the behavior of multiphase flows through detailed mathematical formulations. These models are designed to capture the underlying physical processes and interactions between phases, providing a more comprehensive understanding of flow dynamics.

One of the earliest mechanistic models is the homogeneous flow model (Wallis, 1969) which assumes that all phases are perfectly mixed and flow with the same velocity. This model, while simple, provides a basis for understanding multiphase flow in certain conditions. The separated flow model (Taitel Y. & Dukler A. E., 1976) offers a more detailed approach by treating each phase separately, allowing for different velocities and interactions between phases. The drift-flux model (Hibiki & Ishii, 2003) introduces a drift velocity to account for the relative motion between phases, combining elements of both homogeneous and separated flow models. More complex is the Eulerian-Eulerian and Eulerian-Lagrangian models,

which extend the two-fluid model. The Eulerian-Eulerian model treats each phase as an interpenetrating continuum with its own set of conservation equations, while the Eulerian-Lagrangian model tracks individual particles or droplets within a continuous phase, providing detailed insights into particle dynamics and interactions.

In summary, both empirical and mechanistic models are essential in the study of multiphase flow. Empirical models, with their reliance on experimental data, provide practical correlations that enhance the accuracy of mechanistic models. Mechanistic models, on the other hand, offer a deeper understanding of the physical processes involved. Together, these models enable researchers to develop more accurate and comprehensive descriptions of multiphase flow systems, ultimately leading to improved predictions and better performance in industrial applications.

2.5 Pressure Wave Propagation

The concept of a wave entails the transition from one state to another at a finite velocity (Engelbrecht, 1997). In this context, a state encompasses displacement, particle velocity, stress, deformation, or other quantifiable and observable variables. A wave is characterized as "a disturbance that traverses from one point in a medium to other points at a recognizable propagation velocity." (Durran, 1999).

Pressure waves propagate through a medium, undergo reflection from specific flow constraints within the flow line, and experience attenuation. Waves serve as carriers of energy and momentum, and upon encountering an obstacle, they exhibit reflective behavior concerning the obstacle.

Reflection from a HARD boundary

Consider a wave pulse travelling along a string, progressing from left to right toward a firmly clamped end (Figure 2.5). When the wave pulse approaches the

fixed end, the internal restoring forces, which facilitate the wave's propagation, exert an upward force on the end of the string. However, due to the clamped nature of the end, it remains immobile. As per Newton's third law, the fixed surface exerts an equal downward force on the end of the string. This dynamic engenders a wave pulse from right to left at the same speed and magnitude as the incident wave, albeit with inverted polarity (upside down).

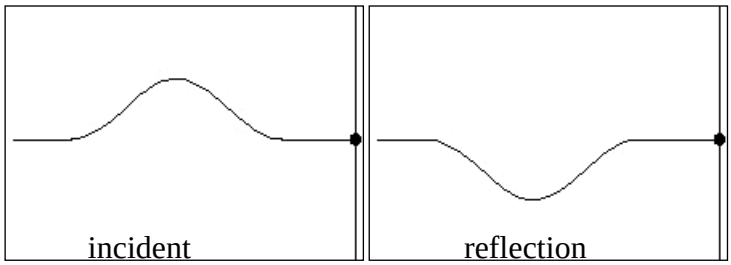

Figure 2.5. At a fixed (hard) boundary, the displacement remains zero and the reflected wave changes its polarity (Russell, 2013)

Reflection from a SOFT boundary

A wave pulse on a string moves from left to right toward the end that is free to move vertically (Figure 2.6). This means that the slope of the string displacement must be zero at the free end, ensuring that the net vertical force at the free end is also zero. Mathematically, this condition is equivalent to the net vertical force being zero. When the wave pulse reaches the free end, it reflects and propagates from right to left with the same speed, amplitude, and polarity (right side up) as the incident wave. At a free (soft) boundary, the restoring force is zero, and the reflected wave has the same polarity (no phase change) as the incident wave

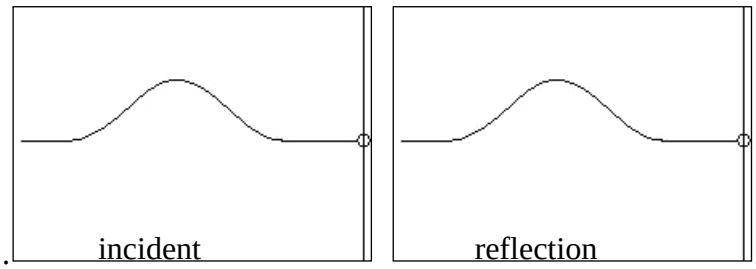

Figure 2.6. At a free (soft) boundary, the restoring force is zero and the reflected wave has the same polarity as the incident wave (Russell, 2013)

Reflection from a discontinuous medium

When a wave encounters a boundary that is between rigid (hard) and free (soft), part of the wave is reflected from the boundary, and part of the wave is transmitted across the boundary. The behavior of reflection and transmission depends on the material properties on both sides of the boundary. One crucial property is the characteristic impedance of the material, which is the product of mass density and wave speed.

In the given cases below, two strings of different densities are connected to have the same tension. The thick string has a density four times that of the thin string. The relationship between the speed of waves on a string and density and tension is determined by:

- From high speed to low speed

  In this case, the incident wave travels from a high wave speed region to a low wave speed region. The amplitude of the reflected wave is less than that of the incident wave, and its polarity changes (Figure 2.7).

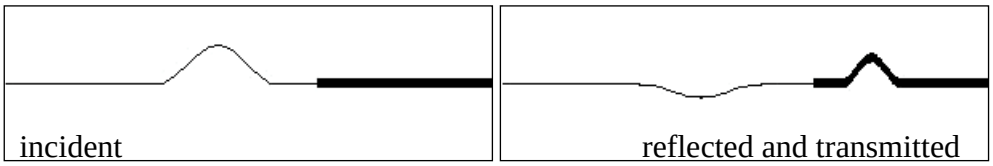

Figure 2.7. At a discontinuity (from high speed to low speed), the reflected wave changes its polarity and decreases its amplitude (Russell, 2013)

- From low speed to high speed

  In this case, the incident wave travels from a low wave speed region to a high wave speed region. The amplitude of the reflected wave is less than that of the incident wave, and has the same polarity. The transmitted wave will have a higher amplitude (Figure 2.8).

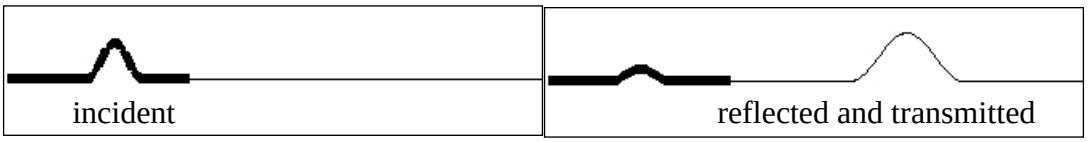

Figure 2.8. At a discontinuity (from low speed to high speed), the reflected wave has the same polarity as the incident wave and decreases its amplitude (Russell, 2013)

The pressure pulse method is a versatile technique that can be used for estimating propagation speed of pressure waves along production lines in multiphase flow conditions with various gas-to-liquid ratios. Moreover, the pressure pulse method can be applied across a wide range of temperature and pressure conditions. As explained above, pressure wave amplitude and polarity change either the velocity varies gradually or it creates discontinuity.

The propagation of pressure waves in multiphase flow in oil production pipelines is a complex phenomenon influenced by various factors. Li (2011) found that the propagation speed of two-phase pressure waves is affected by void fraction, angular frequency, vapor bubble diameter, mass flow rate, and inlet temperature. Ferro (2007) developed a numerical model for multiphase flow in oil production wells, considering different flow patterns and flow properties. Hanafizadeh (2015) experimentally investigated the flow patterns in two-phase oil-water flow, identifying dominant patterns in different pipe inclination angles. These studies collectively underscore the need for a comprehensive understanding of the factors influencing pressure wave propagation in multiphase flow in oil production pipelines.

In the study of Falk, (1999), a comprehensive study on the propagation of pressure pulses in gas-liquid flows within pipelines and wells is conducted. The primary objective of the research was to enhance the understanding of pressure-pulse dynamics in multiphase flow systems, which is critical for improving system

design and preventing accidents in petroleum engineering operations. The study involved the development of a computer program designed to predict rapid pressure transients in gas-oil-water flows. This program utilized a set of homogeneous equations, which were derived and solved using an implicit numerical method. The output from the program included time and position-dependent variables such as pressure, flow velocity, density, void fraction, and sound velocity within a pipe. To validate the computer model, Dr. Falk conducted air-water experiments under atmospheric conditions using both horizontal and vertical loop setups. In the horizontal loop, experiments were performed with a shock-tube, while the vertical loop involved a quick-closing valve at the top. These experiments spanned various void fractions and provided time-series data of pressure and void fraction. The results indicated that the pressure-pulse velocity in dispersed flow was consistent with the theoretical sound velocities in a homogeneous mixture. Additionally, in cases of strong pressure disturbances within separated flow, the pressure pulses behaved similarly to those in dispersed flow.

2.6 Acoustic Velocity

Acoustic velocity, also known as the speed of sound, is a critical parameter in fluid dynamics, significantly impacting various engineering applications such as pipeline transport, hydraulic systems, and petroleum extraction. In single-phase fluids, the speed of sound is relatively well understood and can be accurately predicted using established theoretical models. However, the presence of multiple phases, such as gas-liquid mixtures, introduces complexity that challenges theoretical and empirical approaches.

2.6.1 Acoustic Velocity in Single Phase Flow

The speed of sound in single-phase fluids can be derived from fundamental thermodynamic principles. Initially, Newton proposed that the speed of sound c in an ideal gas is described by:

$$c^2 = \frac{P}{\rho} \tag{2.5}$$

where c [m/s] is the speed of sound, P is the pressure [Pa], ρ is the density [kg/m^3]. The speed of sound is indeed thermodynamic property where subscript S denoting that speed of sound is calculated at isentropic conditions. Newton assumed that air behaves as an ideal gas and that the compressions and rarefactions occurring during sound propagation are slow enough to be isothermal and thermodynamically reversible (White, 1986). However, experimental observations revealed discrepancies between the values predicted by Newton's equation and those measured empirically. Newton himself noted an underestimation of approximately 20%.

Over a century later, Laplace corrected this discrepancy by recognizing that the process should be isentropic rather than isothermal. He revised the speed of sound equation to:

$$c^2 = \frac{\gamma P}{\rho} \tag{2.6}$$

where γ is the ratio of specific heats ($\frac{C_P}{C_V}$), accounting for the adiabatic nature of sound propagation.

This corrected equation, known as the Newton-Laplace equation, provides a crucial link between thermodynamic principles and acoustic measurements.

According to general equations of state, if classical mechanics is used, the speed of sound c for single fluid flow the speed of sound is a variable of the thermal state for isentropic flow it is given by (Lighthill, 1978; White, 1986);

$$c^2 = \frac{\partial P}{\partial \rho}\Big|_s \tag{2.7}$$

The speed of sound is variable and depends on the properties of the medium through which the wave propagates. In fluids, only the medium's compressibility and density are the critical factors.

2.6.2 Acoustic Velocity in Multiphase Flow

Measuring the speed of sound in multiphase flow offers a non-invasive and valuable approach to gaining insights into the fluid's composition, phase distribution, and flow regime within pipelines. Speed of sound measurements can be of principal importance in several areas of petroleum engineering, including pipeline construction, leakage detection, and monitoring deposition and scaling. Additionally, the speed of sound is a critical parameter in predicting the propagation and behavior of acoustic waves in multiphase flow scenarios.

The amplitude of a pulse is influenced by the speed of sound, particularly when the velocity undergoes gradual variations or encounters a discontinuity. This effect can be observed in when a pulse moves from a low-speed region to a high-speed region, resulting in a transmitted pulse with higher pressure (Figure 2.9).

Conversely, as depicted in

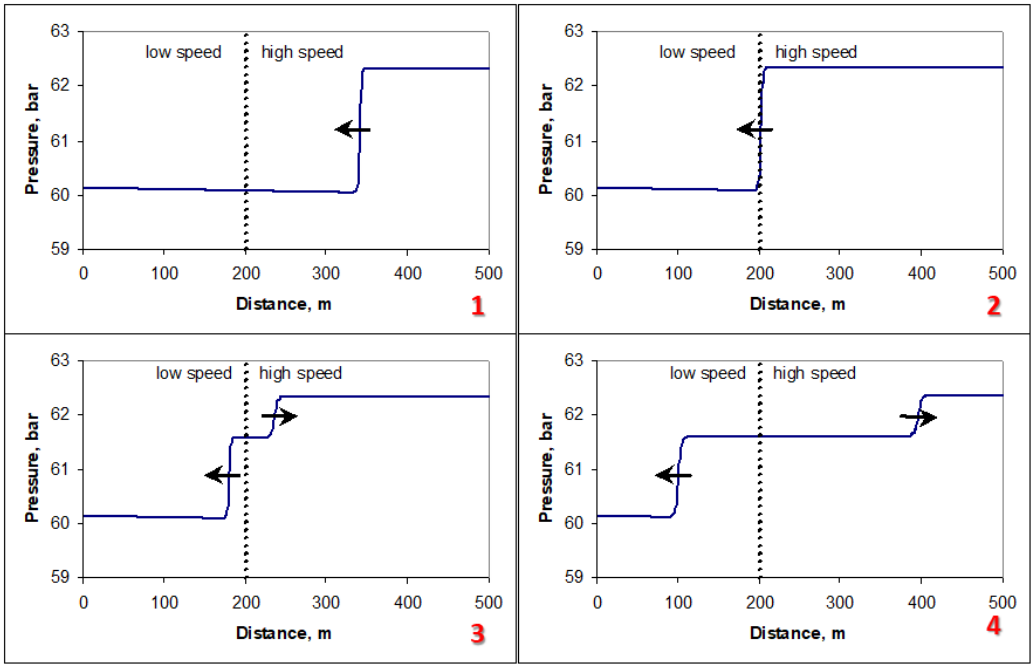

Figure **2.10**, the transmitted pulse exhibits lower pressure when the scenario is reversed. This observation sheds light on why a pressure pulse gains additional amplitude as it travels through a pipe (Falk, 1999).

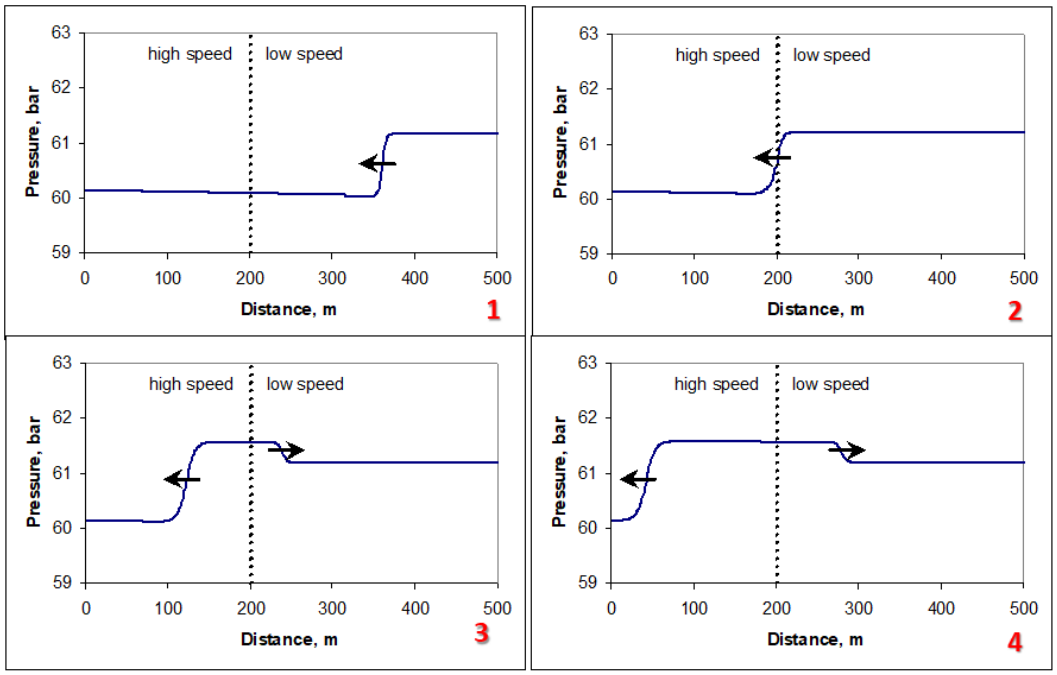

Figure 2.9. Pressure-pulse propagation at discontinuity of speed of sound (from low to high)

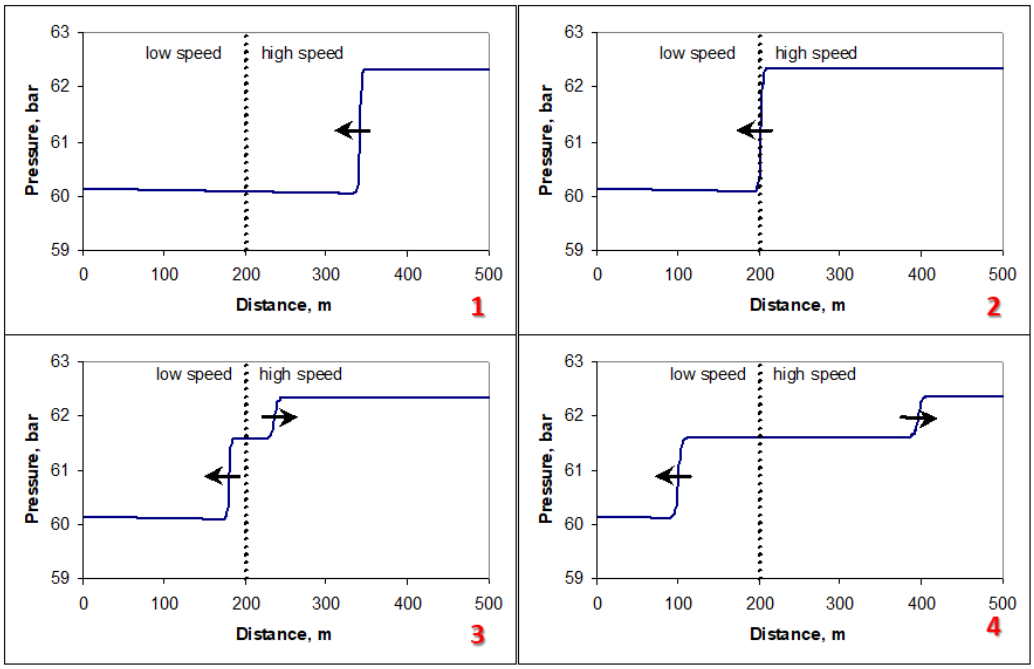

Figure 2.10. Pressure-pulse propagation at discontinuity of speed of sound (from high to low)

Wood's equation is a formula that provides the speed of sound in homogeneous gas-liquid mixtures. It focuses on how changes in the density of the medium affect the velocity of pressure waves (Wood, 1955):

$$c_M{}^2 = \frac{1}{A \times B} \tag{2.8}$$

where,

$$A = [\alpha\rho_G + (1 - \alpha\rho_L)]^{0.5} \tag{2.9}$$

$$B = \left[\left(\frac{\alpha}{\rho_G c_G{}^2}\right) + \left(\frac{1-\alpha}{\rho_L c_L{}^2}\right)\right]^{0.5} \tag{2.10}$$

where α is the void fraction, c is the speed of sound [m/s] in pure phases, ρ is the pure phase density [kg/m^3] and the subscripts G and L shows gas and liquid, respectively. The Wood equation is written for gas and liquid phases only but there exist three phases in this study. Therefore, in order to apply the Wood equation in three phases condition, the density and speed of sound in liquid phase are estimated by using the properties of liquid phases (oil and water) and volumetric fraction of one of the liquid phases:

$$\rho_L = \beta\rho_W + (1 - \beta)\rho_O \tag{2.11}$$

$$c_L = \beta c_W + (1 - \beta)c_O \tag{2.12}$$

where ρ_W and ρ_O are water and oil densities [kg/m^3] at the pressure and temperature of interest, β is the water volumetric fraction.

Henry, R. E. et al. (1971), investigated the dependence of propagation speed on different flow regimes, obtaining analytical expressions for the acoustic celerity in a bubble, slug, and stratified flows. These results also confirmed the more robust

nature of those corrected calculations since their analyses showed that the interfacial drag on a propagating wave is highly dependent on the mode of flow structure through which it passes. Henry derived a model based on slip flow for bubbly flow in high-momentum-fraction two-phase flow, and it is given by the following equation:

$$c_M{}^2 = \frac{\dfrac{1}{\alpha\rho_g + (1-\alpha)\rho_l}}{\dfrac{\alpha}{\rho_g c_g{}^2} + \dfrac{1-\alpha}{\rho_l c_l{}^2}} \tag{2.13}$$

On the other hand, this equation gives closer results to the gas phase for stratified and slug flows. Nguyen et al. (1981) constructed another formulation pressure pulse velocity, which assumes one fluid works as the elastic wall to the other (in stratified flow liquid as an elastic wall for the gas phase):

$$c_M = \frac{\dfrac{1}{\alpha\sqrt{\rho_g} + (1-\alpha)\sqrt{\rho_l}}}{\sqrt{\dfrac{\alpha}{\rho_g c_g{}^2} + \dfrac{1-\alpha}{\rho_l c_l{}^2}}} \tag{2.14}$$

This equation resembles Wood's, but the mixture density calculation is different Figure 2.11.

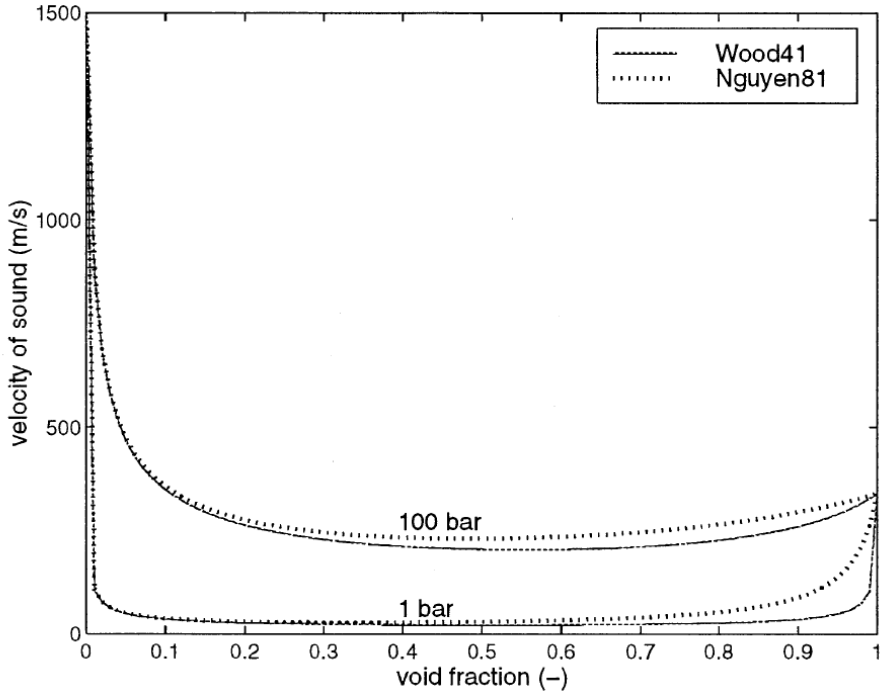

Figure 2.11 Comparison of pressure pulse velocity results from Wood (1955) and Nguyen et al. (1981) at 1 bar and 100 bar homogeneous air-water flow.

Dong and Gudmundsson (1993) developed a mathematical model to compute the sound velocity of a gas-oil-water mixture at a known temperature and pressure using the properties of gas, oil and water directly under homogeneously mixing conditions. They proposed the following equation to calculate the speed of sound:

$$c_M{}^2 = \frac{\left(xC_{pG} + (1-x)\left[yC_{pW} + (1-y)C_{pO}\right]\right)/(xC_{vG} + (1-x)[yC_{vW} + (1-y)C_{vO}])}{(\alpha\rho_G + (1-\alpha)[\beta\rho_W + (1-\beta)\rho_O])(\alpha K_G^T + (1-\alpha)[\beta K_W^T + (1-\beta)K_O^T])} \quad (2.15)$$

where ρ's, C_P's, C_V's and K^T's are density, isotropic, volumetric specific heats [J/(kg·K)] and isothermal compressibility of each phase and the subscripts G, O and W stand for gas, oil and water phases, respectively. x is the gas-liquid mass fraction, y is the water-oil mass fraction, α is the gas-liquid void fraction, and β is the water-oil volumetric fraction. As stated, the speed of sound in a gas-oil-water mixture is directly related to the density, compressibility and specific heat of each

phase in the mixture, which is calculated from properties using correlations and PVT models based on the equation of states as stated by (Dong & Gudmundsson, 1993b).

2.7 Numerical Models

Numerical models in multiphase flow are essential tools that utilize computational techniques to simulate and predict the behavior of complex fluid systems involving multiple phases. These models are grounded in the fundamental equations of fluid dynamics and thermodynamics, providing detailed insights into flow dynamics and phase interactions unlike empirical models.

The volume of fluid (VOF) model simulates free surface and interfacial flows where phases are immiscible, using numerical representation of fluid interfaces with volume fractions within computational cells. It is valuable for studying phenomena like wave breaking, sloshing, and multiphase flow in industrial and environmental applications. The discrete element method (DEM) is a numerical technique that simulates the behavior of individual particles, particularly in granular or particulate flows within a fluid medium. It tracks motion, collisions, and interactions between discrete particles using Newtonian mechanics principles, enabling detailed studies of particle dynamics and their influence on overall flow behavior.

In addition, Computational Fluid Dynamics (CFD) methods integrate various multiphase flow models, such as Eulerian-Eulerian, Eulerian-Lagrangian, and VOF models, to simulate complex multiphase flow phenomena. These models are embedded within CFD software packages offering powerful tools for analyzing and optimizing industrial processes involving multiphase flows. OLGA can be given as a numerical CFD software package that uses for commercial purposes in oil and gas industry (Schlumberger, 2019). In the study of Bendlksen et al., (1991) an explicit first order finite difference scheme and focused on the theoretical

foundations of OLGA's dynamic two-fluid model. This model treats gas and liquid phases as separate continua, incorporating conservation equations for mass, momentum, and energy. It considers phase interactions, phase transitions (such as bubble formation and collapse), and the effects of flow regime transitions.

Numerical models in multiphase flow continue to evolve with advancements in computational techniques and increased computing power. They play a crucial role in advancing our understanding of multiphase flow phenomena and their applications across diverse industries, from energy and manufacturing to environmental and biomedical engineering.

2.7.1 Modeling of Pressure Wave Propagation in Multiphase Flow

Modeling of pressure wave propagation in multiphase flow is the main focus of this study. It is used to measure the propagation speed of pressure waves in multiphase flow, which offers a non-invasive and valuable approach to gaining insights into the fluid's composition, phase distribution, and flow regime within pipelines. propagation speed of pressure wave measurements can be of principal importance in several areas of petroleum engineering, including pipeline construction, leakage detection, and monitoring deposition and scaling. Additionally, the propagation speed of pressure waves serves as a key parameter in predicting the propagation and behavior of acoustic waves in multiphase flow scenarios. Estimating the propagation speed of pressure waves in multiphase fluid flow by observing pressure waves generated during normal operations is related to the speed of sound in single and multiphase flow conditions.

Ünalmis (2016) investigates into the application of sound speed in flow measurement within high-pressure/high-temperature downhole environments. The study underscores the inherent challenges in employing sound speed for flow measurement, attributed to the intricate dynamics of flow patterns and the variability in phase fractions. To address this complexity, the research conducts

multiple flow loop tests aimed at directly assessing the viability of sound speed in flow rate measurement. The findings from these tests are subsequently correlated with real-life field examples, providing valuable insights into the practical applicability of sound speed measurements in such demanding operational conditions.

The study by Fu et al., (2020), introduces an approach for the direct numerical simulation of the speed of sound in compressible two-phase flow, utilizing a stratified multiphase flow model. This simulation framework incorporates frequency, volume fraction, viscosity, and heat transfer effects considerations. Through a comparative analysis with experimental data, the simulations demonstrate a commendable agreement. The study discerns that in air-water bubbly two-phase flow, the speed of sound tends to be higher at elevated frequencies. Additionally, it notes that the homogeneous condition is more effectively satisfied at lower frequencies concerning phasic velocities, and the wave propagation exhibits an isothermal bubble behavior.

Most models for two-phase flow are typically based on isothermal conditions, as proposed in the study conducted by Kieffer (1977). However, further advancements in modeling techniques are being pursued to account for non-isothermal scenarios and the varying properties of fluids in multiphase flow. This evolving research is instrumental in refining our understanding of the complexities of multiphase flow phenomena and enhancing the accuracy of prediction models.

The calculation of the speed of sound in multiphase flow requires a particular examination of the properties of each phase within the fluid. Empirical equations or experimental data are commonly employed to determine each phase's specific heat, density, and compressibility. Dong & Gudmundsson, (1993a&b) proposed a method for estimating the speed of sound using these properties, thereby providing a valuable tool for predicting acoustic velocity in various multiphase flow scenarios. The calculated sound velocity is compared with measured data in two-

component systems, indicating that the propagation of sonic waves in gas-liquid mixtures is generally isentropic. The paper highlights the practical importance of understanding sonic wave propagation in multiphase mixtures in various petroleum engineering applications.

A conceptually innovative approach was introduced by Godunov, (1959) who solved the Riemann problem forward in time. The Riemann problem is named after the German mathematician Bernhard Riemann. The problem typically arises in the study of hyperbolic systems of conservation laws, which can describe various physical phenomena, including shock waves, rarefaction waves, and contact discontinuities. It entails solving a hyperbolic system of conservation laws using initial data with a discontinuity. This method fundamentally changed how numerical solutions for fluid dynamics problems were approached. Godunov's method involved using exact solutions to the Riemann problem at each cell interface, leading to the accurate capturing of shock waves and discontinuities in the flow. This approach laid the groundwork for the development of high-resolution shock-capturing schemes.

Building on Godunov's foundational work, Roe (1981) developed an approximate Riemann solver. Roe's method offered a more practical implementation by simplifying the exact solution process, making it computationally more efficient while retaining high shock wave resolution accuracy. Roe's solver approximates the solution by linearizing the nonlinear hyperbolic equations, significantly reducing computational complexity and making it a widely adopted technique in CFD.

Romate, (1998) applied an approximate Riemann solver to a set of hyperbolic two-fluid equations, explicitly addressing the complexities of multiphase flows. Their work demonstrated how this solver could effectively handle the interactions between different fluid phases, such as gas and liquid, typical in industrial applications like chemical reactors and petroleum extraction. By accurately

predicting the behavior of multiphase flows, this approach helps in optimizing design and operation processes in various engineering fields.

Zhou & Adeeumi (1996) extended the application of approximate Riemann solvers to the modeling and simulation of transient two-phase flow in natural gas pipelines. This application was particularly significant because it addressed the real-world challenge of predicting the dynamic behavior of gas and liquid phases in pipelines, which is crucial for the efficient and safe transport of natural gas. Their work provided a robust tool for pipeline engineers to analyze and mitigate issues such as pressure surges and flow instabilities.

LeVeque (1992) presented a comprehensive theory behind approximate Riemann solvers, providing a detailed explanation of the mathematical and computational techniques involved. LeVeque emphasized the importance of understanding wave propagation processes in the flow, which are central to the accuracy and effectiveness of these solvers. The book outlined the advantages of these methods, including their ability to minimize numerical diffusion and oscillation, which are common problems in CFD simulations. Moreover, LeVeque highlighted the straightforward extension of these solvers to second-order accuracy, enhancing their precision without significantly increasing computational effort.

Despite their advantages, LeVeque (1992) acknowledged the complexities involved in using and modifying approximate Riemann solvers. These methods require the governing equations to be in conservation form, which can be a significant constraint in some applications. Additionally, implementing these solvers can be intricate, demanding a deep understanding of both the mathematical theory and the physical phenomena being modeled.

To address some of these challenges, LeVeque (1997) He developed a scheme for more general partial differential equations (PDEs) for single-phase flow. He created a software package called CLAWPACK, which implements algorithms for high-resolution multidimensional wave propagations with hyperbolic systems. This

extension broadened the applicability of Riemann solvers beyond conservation laws to a broader range of fluid dynamics problems, including those involving complex geometries and boundary conditions.

The study of Shyue (2010) describes a simple mapped grid approach for efficient numerical simulation of compressible multiphase flow in general multi-dimensional geometries using the 2D and 3D versions of the CLAWPACK software package. It employs a standard high-resolution mapped grid method in wave-propagation form and presents numerical results to validate the approach. The technique allows for extension from two to three dimensions and assumes minor physical effects such as viscosity, surface tension, and heat conduction. The paper also demonstrates good agreement as the mesh is refined and presents a specific example involving simulating a shock wave in liquid over-dispersed phases in a cylindrical nozzle.

CHAPTER 3

STATEMENT OF THE PROBLEM

In the oil and gas industry, the efficient and safe transportation of multiphase flows through pipelines is a critical challenge due to the complex interactions between different phases of the fluid, such as gas, oil, and water. Pressure wave propagation within these multiphase flows plays a crucial role in understanding fluid flow behavior, influencing key factors such as phase distribution, flow regime, and pipeline integrity. Despite the significance of pressure wave dynamics, current models often fail to accurately predict the speed of pressure waves and their effects on fluid behavior, particularly under varying operational conditions.

Empirical models like the Wood model and the Dong and Gudmundsson model have been widely used to estimate the speed of sound in multiphase flows, yet discrepancies between these models and actual field measurements often arise, leading to challenges in their practical application. Additionally, numerical models such as 1-D and 2-D simulations offer potential insights into pressure wave behavior, but they are frequently limited by their assumptions and complexity, which can prevent accurate predictions of wave propagation and amplitude changes.

The lack of a reliable, comprehensive approach to accurately model and predict pressure wave propagation in multiphase flows presents a significant gap in the current body of knowledge. This gap not only limits the ability to optimize pipeline operations but also poses risks to the safety and integrity of the pipeline infrastructure.

This research aims to address these challenges by developing a robust method for accurately determining pressure wave speeds in multiphase flows, comparing

empirical models with field data, and refining numerical simulations to better represent the complex dynamics of multiphase flow in pipelines. The ultimate goal is to enhance the predictive capabilities of pressure wave modeling, thereby contributing to more efficient and safer pipeline operations in the oil and gas industry.

CHAPTER 4

MATERIALS AND METHODS

4.1 Field Measurements

The field data consists of pressure measurements, separator production rates, GOR and water cut values, and the average oil/gas gravities produced from four wells during a testing campaign conducted on an offshore production platform in Norway. All four producer wells were part of a reservoir undergoing water alternate gas injection (WAG) treatment, wherein the injectors alternately changed from gas to water injection at specific intervals. Pressure signals were recorded schematically using the setup located on the platform, as shown in Figure 4.1.

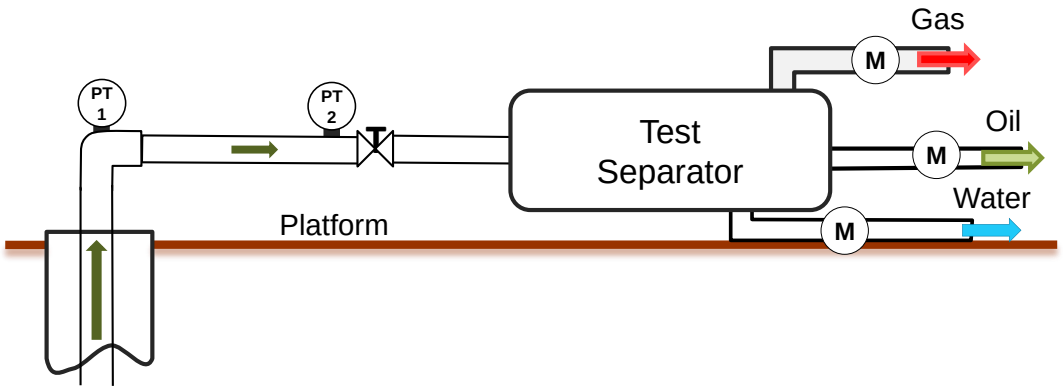

Figure 4.1. Schematic diagram of measurement setup on an offshore platform having a three-phase separator to evaluate propagation speed of pressure waves along the production line using pressure transmitters.

There are two pressure transmitters; one pressure transmitter was placed at the wellhead, and the second transmitter was placed on the choke, measuring the upstream pressure. These transmitters were connected to the data logger. The production test line reaches a three-phase separator. The distances between the two transmitters are 30 – 35 m, varying for each well.

Each time a well was tested in the test separator, the pressure data were recorded. This involved logging signals from all transmitters simultaneously in 2-minute data sets, which were then stored along with each phase's corresponding production flow rates measured through the three-phase test separator. The four wells cover a wide range of pressure, GOR and water cuts, and since all wells were within the WAG area, the variations in each well over time were significant. The production test data from the test separator are presented in **Table A - 1** in Appendix.

When a well was tested using the test separator, the measured pressure data from the wellhead and choke were analyzed to determine the propagation speed of pressure waves in the fluid. The test data were grouped based on the wellhead pressure ranges (Table A - 4 to **Table A - 7**).

4.1.1 Void Fraction Calculations

The void fractions of each production test data are calculated from the measured rates by the ratio of the volume of gas to the volume of the mixture at the in-situ condition.

The void fraction under no slip condition is defined as follows:

$$\alpha = \frac{V_g}{V_g + V_l}, \tag{4.1}$$

where V_g and V_l are in-situ volumes [m^3] of gas and liquid phases at the pressure and temperature of interest. These volumes are obtained from the field data. The gas gravity and API gravity of oil, separator water cut (WC), and GOR [Sm3/Sm3]) are given in the field data. The formation volume factors of each phase at the given pressure and temperature are calculated from the fluid properties, and then the in-situ void fraction is calculated as follows:

$$\alpha = \frac{B_g GOR}{B_g GOR + B_o + \frac{WC}{1 - WC} B_w}. \quad (4.2)$$

where the gas formation volume factor [m^3/Sm^3] B_g is estimated by solving real gas equation of state suggested by Lee and Kesler (1975), the oil formation volume factor [m^3/Sm^3] B_o by the Standing correlation, the water formation volume factor [m^3/Sm^3] B_w by the McCain method. The void fraction value calculated from this equation will be used to plot the void fraction versus the propagation speed of pressure waves measured by analyzing pressure signals.

4.1.2 Pressure Wave Propagation Speed Measurement Method

Measured pressure data is analyzed by cross-correlation method to estimate pressure wave propagation speed. Cross-correlation is a statistical measure used to evaluate the similarity between two waveforms, specifically pressure fluctuations along a pipe, as a function of a time lag. This method involves calculating the time-lag component and applying it to one of the two assessed signals proportionate to the signals' time intervals. Cross-correlation is widely applicable across various fields, including signal pattern recognition, matching shorter signals within longer ones, particle analysis, neurophysiology, and cryptanalysis. Its primary application in this context is determining the time delay between two signals, which is the focus of this method. (Hanson et al., 2008)

In practical terms, cross-correlation works by shifting one signal in time relative to another and calculating a correlation coefficient at each time shift. The time lag that maximizes the correlation coefficient indicates the delay between the two signals. This technique is beneficial in fluid dynamics and pipeline monitoring, where understanding the propagation of pressure waves can provide insights into flow characteristics and potential anomalies within the pipeline system.

Cross-correlation is a well-established method for comparing the properties of two signals, measuring similarities between them as a function of the time lag of one relative to the other, and represented as follows:

$$R(\tau) = \int_{-\infty}^{+\infty} x(t)y(t+\tau)dt \tag{4.3}$$

where $x(t)$ and $y(t)$ are a function of time, τ is a time delay and $R(\tau)$ is cross-correlation. In this study, recorded pressure signal readings in two different transmitters from a horizontal pipeline are analyzed by cross-correlations, and the time delays are computed by a developed MATLAB code using the script function *xcorr*.

The pressure wave propagation speed is calculated from:

$$c_M = \frac{L_P}{|\tau|} \tag{4.4}$$

where L_P is the length of the pipe and τ is a time delay of the signals obtained from cross-correlation. It should be noted that the propagation speed of pressure waves is not exactly the same as the speed of sound which is a thermodynamic property (estimated by the empirical equations given in Eqn. (2.8) and Eqns. (2.13-2.15) which are assuming homogenous mixing and no-slip conditions), and it represents the propagation velocity of small pressure perturbations.

Two pressure signals were recorded at a frequency of 2000 Hz using two pressure transmitters, one located at the wellhead and the other upstream of the choke, as shown in Figure 4.2. A Butterworth filter with a cut frequency of 10 Hz and order of 5 is applied to the data obtained from each well at different measurement test. Filtered data is used for cross-correlation analyses. Figure 4.2 presents a plot of measured raw pressure data for two signals and their corresponding filtered signals from a well measurement test. In the plot, the red line represents the pressure data

from the first transmitter at the wellhead, while the blue line represents the data from the second transmitter at the choke upstream. The pressure differences between the two signals are low. Additionally, there was no valve action during the interval of data acquisition. The waves are considered to be generated by natural disturbances through the wellbore and flowline.

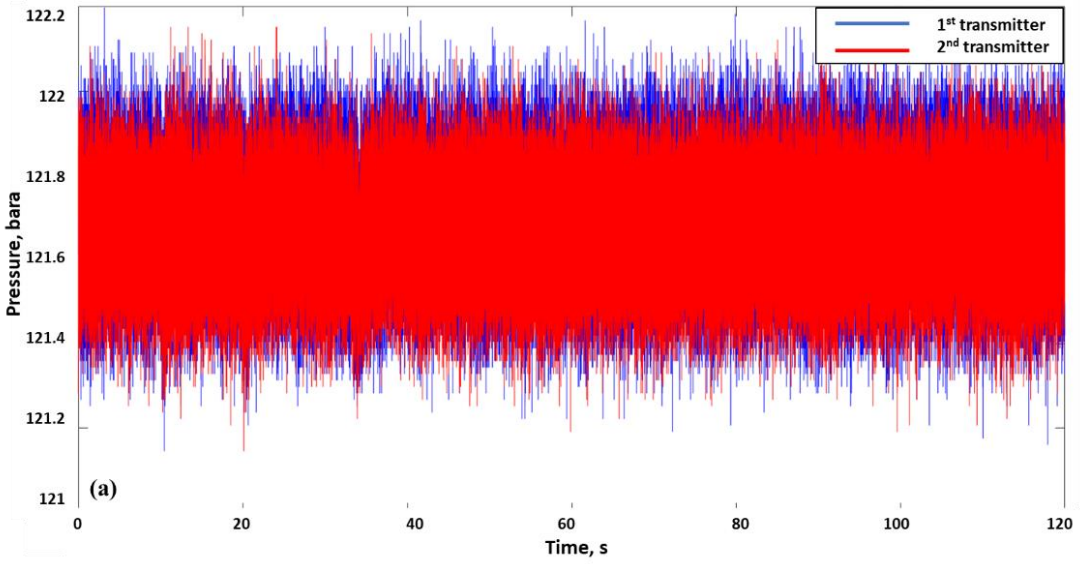

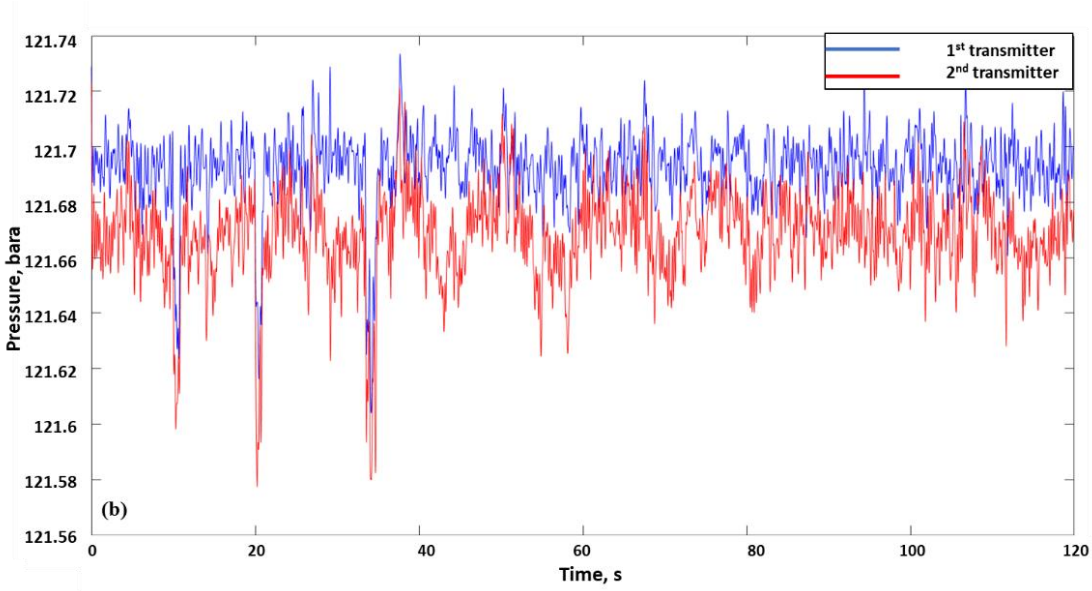

Figure 4.2. Two pressure signals recorded by transmitters in well W-2 during test #6 a) without filter and b) after data filtering.

The pressures were continuously recorded for two minutes at the specified frequency. Subsequently, the recorded data was analyzed using a shifting time-window approach. Each window of data to be evaluated spans a period of 10 seconds through measurements (for example, the first window covers measurements from 0 to 10 seconds, the second window from 10 to 20 seconds, and so forth). Cross-correlations were then applied to each shifting window.

In Figure 4.3, an example of a time interval for two signals. As observed, the waves are detectable, and the time lag between two peaks is significant. Since the pressure wave reaches the first transmitter later than the second transmitter after a specific time, it can be concluded that the pressure waves were generated at the downstream side of the flowline and propagated toward the upstream. The cross-correlation method is used to calculate the time delay between these signals. The values of $R(\tau)$ and τ are computed for each recording from the two transmitters. When the pressure recording for the given interval is analyzed, the time delay is calculated as 0.1895 s and $R(\tau)$ is around 0.94 (see Figure 4.4).

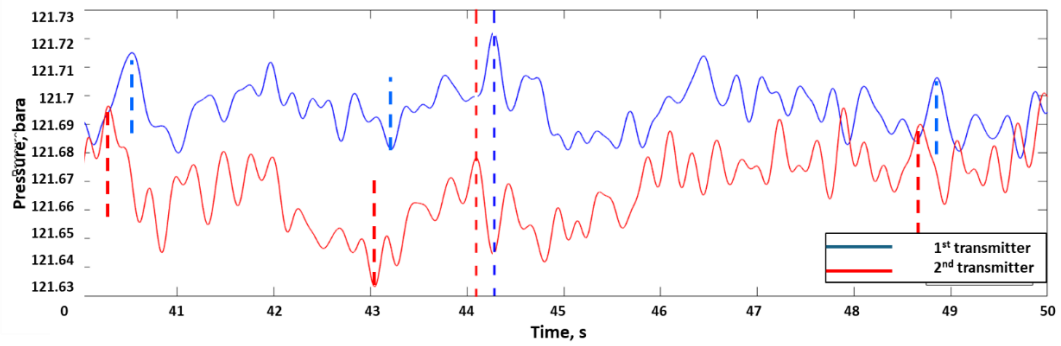

Figure 4.3. Two pressure signals obtained by transmitters from the test W-2/6 between 40s and 50s.

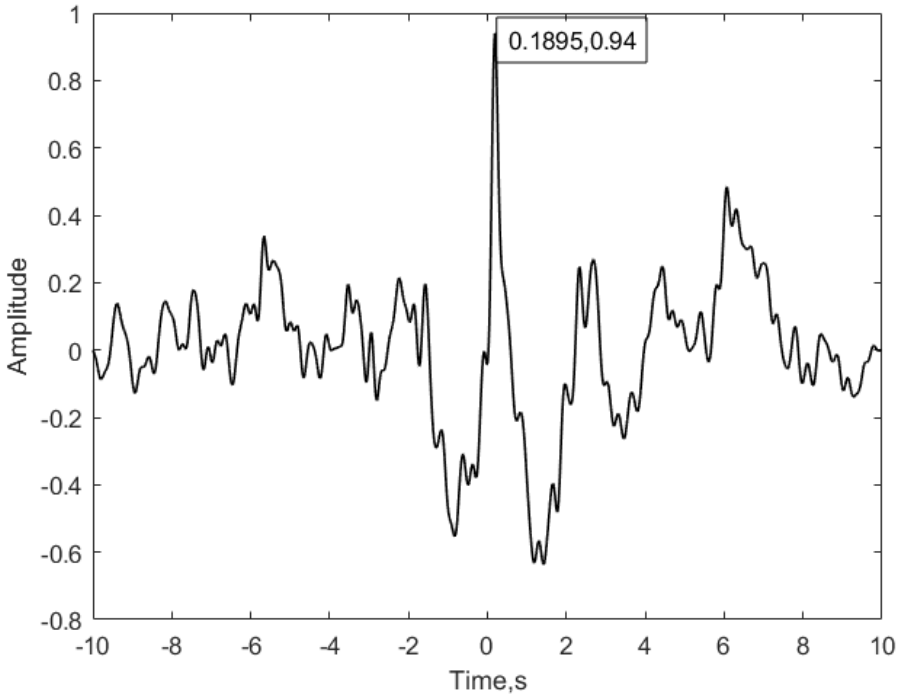

Figure 4.4. Cross-correlation for the recorded pressure signals from the test W-2/6 between 40s and 50s.

4.2 Pressure Wave Velocity Estimation Simulator

The Fortran-based computer program developed by Markland called Hastenn is a well-known reference in petroleum engineering and natural gas processing. This work involves the development of computational tools to predict the physical properties of natural gases accurately. These properties include but are not limited to, density, viscosity, compressibility factor, and acoustic velocity, which are critical for the design, operation, and optimization of natural gas production and transportation systems.

In this study, Hastenn is used to compare the propagation speed of pressure waves results from both cross-correlation and numerical models. The detailed explanation

for acoustic velocity calculation can be found below for the computer program (Parlaktuna & Gudmundsson, 1991).

Acoustic velocity calculations are based on as the Eqn (2.7) at isentropic conditions. Velocity of each phase is estimated separately, for gas phase by using the definition of compressibility at isentropic conditions, K^S

$$K^S = \frac{1}{\rho}\frac{dP}{d\rho}\Big|_S \tag{4.5}$$

where density of gas is calculated from real gas equation, and for compressibility factor the Lee-Kessler method (1975) is used and eventually, the relationship in Eqn (2.7) results.

The relation between isothermal (K^T) and isentropic compressibilities is given as:

$$\frac{K^S}{K^T} = \frac{C_v}{C_p} \tag{4.6}$$

and K_T is defined as:

$$K^T = \frac{1}{\rho}\frac{dP}{d\rho}\Big|_T \tag{4.7}$$

In addition, isentropic compressibility of brine is a function of pressure, temperature and salinity and based on Rowe and Chou (1970) correlation and isobaric heat capacity is calculation relies upon the study of Michaelides (1981). On the other hand, acoustic velocity of oil depends on the empirical tables and the program calculates it for the given API gravity of the oil. Basically, the acoustic velocity of the mixture is estimated from the homogeneous properties of the fluid as:

$$\begin{aligned} K^T_{Mix} &= \alpha K^T_G + (1-\alpha)K^T_L \\ \rho_{Mix} &= \alpha\rho_G + (1-\alpha)\rho_L \end{aligned} \tag{4.8}$$

$$c_{Mix} = \sqrt{\frac{\frac{C_{pmix}}{C_{vmix}}}{\rho_{Mix} K_{Mix}^{T}}}$$

The values obtained from Eqn (4.2) with a range of void fraction 0 to 1, are compared with the cross-correlation results.

4.3 Numerical Modeling of Pressure Wave Propagation

In this study, in order to model the pressure wave propagation, OLGA modeling, 1-D numerical model and 2-D numerical model are used. The following sections will provide methods of the analysis.

4.3.1 OLGA Modeling

OLGA model in a Dynamic Multiphase Flow Simulator OLGA (OiL & GAs) (Schlumberger, 2019) is a dynamic multiphase flow simulator utilized throughout the oil and gas industries to investigate transient flow elements in wellbores and pipelines. Originally developed by the Institute for Energy Technology (IFE) in Norway in the early 1980s, OLGA has since become an invaluable tool in predicting how multiphase flows will interact for various operating conditions.

The OLGA employs a comprehensive three-fluid model incorporating distinct continuity equations for gas, oil (or condensate), and water liquids. Additionally, separate continuity equations are utilized for oil (or condensate) and water droplets. These various fluid phases can interact through interfacial mass exchange, allowing for a dynamic coupling of their properties. The OLGA model involves the solution of a total of seven conservation equations. These consist of three equations for mass, addressing the diverse fluid phases, three equations for momentum, capturing

the dynamic behavior of the system, and one equation for energy. In addition to these conservation equations, there's one equation of state focusing on pressure.

OLGA's simulation capabilities are built on advanced numerical methods and physical models that accurately represent multiphase flow dynamics. The primary methodologies employed in OLGA include:

- Dynamic Two-Fluid Model: The dynamic two-fluid model forms the cornerstone of OLGA. This model treats the gas and liquid phases as interpenetrating continua, each governed by its own set of equations for mass, momentum, and energy conservation. The continuity equations ensure mass conservation for each phase, while the momentum equations account for the forces acting on each phase, and the energy equations ensure energy conservation. The equations include terms for interphase interaction forces, stress tensors, and heat flux, which are critical for accurately capturing the complex interactions between phases.
- Finite Volume Method (FVM): OLGA utilizes the Finite Volume Method to discretize the governing equations over a computational grid. This involves dividing the pipeline or wellbore into small control volumes or cells, converting the partial differential equations into algebraic equations using integral forms over each control volume, and solving these equations iteratively to obtain the flow field.
- Equation of State (EOS): An Equation of State (EOS) describes the thermodynamic properties of the gas and liquid phases. OLGA typically employs the Peng-Robinson EOS or the Soave-Redlich-Kwong EOS to calculate phase behavior and properties such as density, compressibility, and phase equilibrium.
- Heat Transfer Models: Heat transfer between the fluid and the surrounding environment, as well as between phases, is modeled using principles of conduction, convection, and radiation. These models help predict temperature profiles and thermal stresses in pipelines and wellbores.

This modeling approach creates the field measurement setup in the OLGA modeling environment with a slight modification. As in the field, the first pressure transmitter is located just after the inlet point, representing the wellhead. The inlet point is connected to a horizontal pipe, further connected to a valve to generate artificial pressure disturbances, mimicking natural pressure fluctuations. Note that there was no valve action in this field measurement campaign. The second transmitter is placed just upstream of the valve. The schematic diagram of OLGA simulations is shown in Figure 4.5.

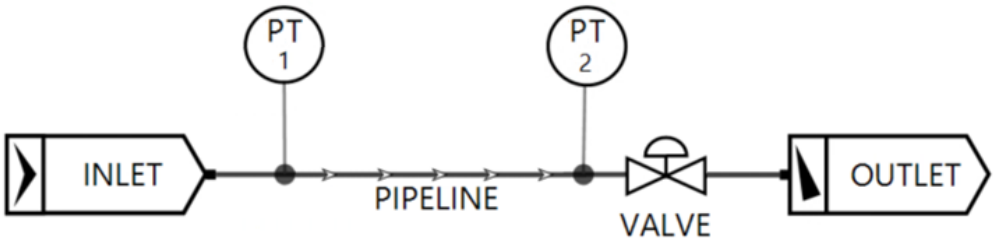

Figure 4.5. Schematic diagram of OLGA simulations for field measurements

For each grouped dataset given in Table A - 4 to Table A - 8, each group's average total liquid flow rate values are used as input for the transient simulations along with the specified wellhead pressure and temperature, which are the pressure grouped values of the datasets. Since only the gravities of the produced phases are available (not the compositional data), the black-oil phase behavior model is applied in the OLGA simulation. The spatial and temporal discretization in OLGA simulations are 1 meter and 0.0005 seconds respectively. The time step is deliberately set to match the data acquisition frequency of 2000 Hz. The grid size is arranged so that CFL condition will be satisfied, and the CFL number will be well below unity with expected the propagation speed of pressure waves. With the average total liquid flow rate, the void fraction is adjusted by changing the GOR to observe the behavior of the propagation speed of pressure waves as a function of the void fraction at each grouped wellhead pressure.

The valve generated artificial pressure disturbances in each simulation to simulate natural pressure fluctuations, mimicking real-world conditions. The simulations

were conducted with exemplary time steps, ensuring accuracy, and the resulting pressure values at transmitter locations were recorded. Subsequently, the recorded pressure data were analyzed to identify the peak points on the pressure signals, as shown in Figure 4.6.

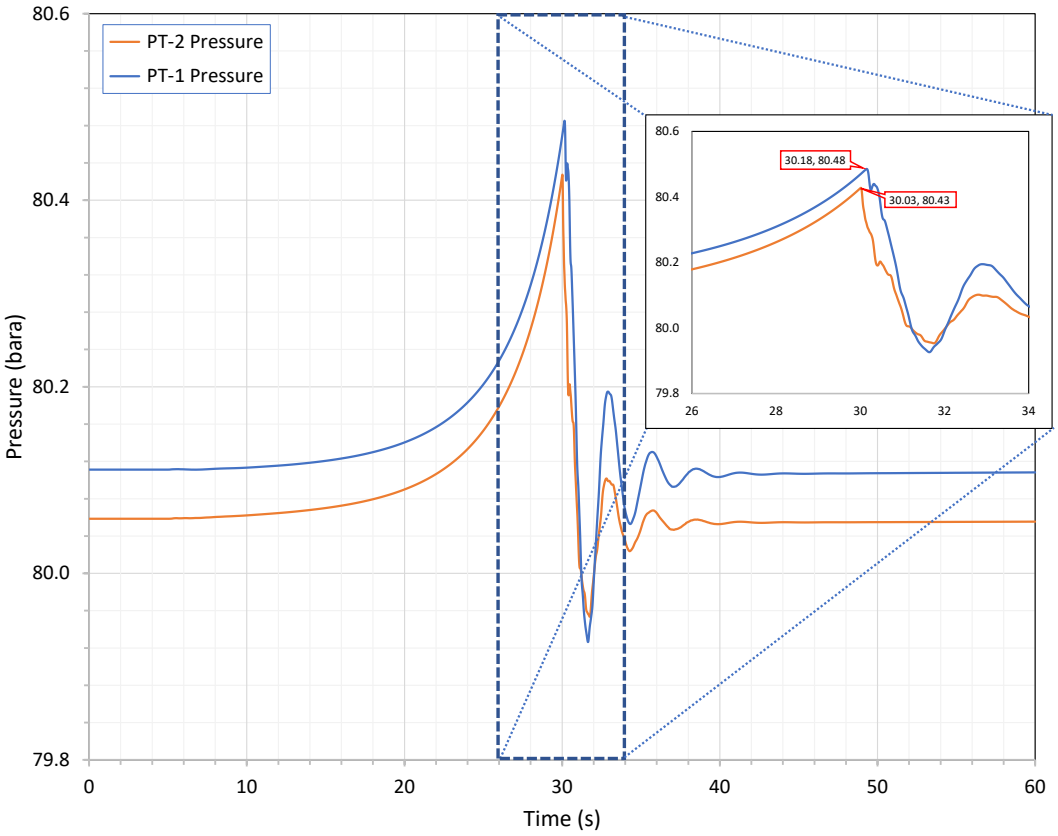

Figure 4.6. An example plot of OLGA simulation results.

Using this information, the time of flight of the pressure wave was calculated to determine the wave propagation speed. This speed is indeed the effective propagation speed of pressure waves in the simulated environment. These simulations were repeated for a range of void fractions by changing the GOR at each grouped data wellhead pressure value.

4.3.2 1-D Modeling

The computer program Markland developed that utilizes the CLAWPACK software package to profile deposits and debris in oil and gas pipelines is used as a 1D numerical model in this study. The basis of this method is to make use of pressure waves created by sudden valve action, and the pressure wave propagation provides possible position and thickness of the deposition through the pipe for single-phase flow.

The single-phase model was adapted to handle multiphase flow by integrating modifications that account for the presence of different phases within the computational domain in this study. This approach is grounded in the concept of effective property methods, where the physical properties of the single-phase model, such as density and viscosity, are adjusted to reflect the averaged or effective properties of the multiphase mixture.

The basis of the mathematical model of single-phase flow in a pipeline is defined with partial differential equations as a transient process. The flow of viscous single fluid is described with mass and momentum balance equations and shown below, respectively:

$$\frac{\partial(A\rho)}{\partial t} + \frac{\partial(A\rho v)}{\partial x} = 0 \tag{4.9}$$

$$\frac{\partial(A\rho v)}{\partial t} + \frac{\partial(A\rho v|v|)}{\partial x} + \frac{\partial(Ap)}{\partial x} = -\frac{f}{2D}\rho v|v|A + \frac{4}{3}\frac{\partial}{\partial x}\left(A\mu\frac{\partial v}{\partial x}\right) - A\rho g\frac{dz}{dx} \tag{4.10}$$

where $v = v(x,t)$ is the cross-sectional average fluid flow velocity in the direction x (along the pipe) and at the time t, $p = p(x,t)$ the pressure, $\rho = \rho(x)$ the fluid density, μ the dynamic viscosity of the fluid, $D = D(x)$ the flow diameter, $A = A(x)$ the flow area, g the acceleration of gravity, and z is the opposite direction of gravity. Since the equations are for transient flow, heat transfer can be neglected and behave like isothermal flow.

As described in Eqn (2.7), the pressure transients (the pressure waves generated by the valve action) in a fluid-filled pipe propagate with the in-situ speed of sound.

By combining the definition of speed of sound Eqn (2.7) and introducing the mass flow as $m = \rho v$ and neglecting the viscous term since the second derivative of flow velocity is much smaller than the other terms, the Eqns (4.18) and (4.19) transform to:

$$\frac{\partial p}{\partial t} + \frac{c^2}{A}\frac{\partial (m)}{\partial x} = 0 \tag{4.11}$$

$$\frac{\partial m}{\partial t} + \left(1 - \left(\frac{v}{c}\right)^2\right) A \frac{\partial p}{\partial x} + 2v\frac{\partial m}{\partial x} = -\frac{f}{2DA}\frac{m|m|}{\rho} - A\rho g\frac{dz}{dx} \tag{4.12}$$

These equations are first-order hyperbolic PDEs that investigate the pressure wave propagation through a pipeline with the dependent variables of p and m in 1-D.

The system of equations can be written in a matrix form and compact form, shown below in Eqns (4.22) and (4.23):

$$\frac{\partial}{\partial t}[q] + [B]\frac{\partial}{\partial x}[q] = [S] \tag{4.13}$$

$$q_t + Bq_x = S \tag{4.14}$$

where q is the vector of the state variables, B is the coefficient matrix for the spatial derivatives of the state variables, and S, is referred to as "source term" representing impulsive or continuous imposed variations in the state variables. The full form of q, B and S are defined as;

$$q = \begin{bmatrix} p \\ m \end{bmatrix} \quad B = \begin{bmatrix} 0 & c^2 \\ 1 - (v/c)^2 & 2v \end{bmatrix} \quad S = \begin{bmatrix} 0 \\ -\frac{f}{2DA}\frac{m|m|}{\rho} - A\rho g\frac{dz}{dx} \end{bmatrix} \tag{4.15}$$

The numerical solver CLAWPACK (Conservation LAWs PACKage) available in web (LeVeque, 1995), is used to solve the system of partial differential equations that describes the propagation of pressure pulse. It applies finite volume methods to solve time-dependent hyperbolic systems of equations.

LeVeque (1997) developed a set of high-resolution multi-dimensional wave propagation algorithms for general time-dependent hyperbolic systems. These methods were based on solving Riemann problems and applying limiter functions to the resulting waves. For non-linear systems of conservation laws, the methods are conservative and provide excellent shock resolution. LeVeque also extended the methods to certain hyperbolic systems that are not in conservation form and to problems with capacity function.

The Riemann problem involves a one-dimensional system of conservation laws. The initial condition for the Riemann problem is a piecewise constant function with a single discontinuity:

$$u(x,0) = \begin{cases} u_L, & x < 0 \\ u_R, & x \geq 0 \end{cases} \tag{4.16}$$

where u_L and u_R are constant states to the left and right of the discontinuity, respectively.

CLAWPACK is designed to handle time-dependent hyperbolic systems of standard conservation laws in 1, 2, and 3 space dimensions. When working in one-dimensional space, the package is capable of solving a system of equations in the form of (Leveque, 2006);

$$\kappa(x)q_t + f(q)_x = \psi(q,x,t) \tag{4.17}$$

where $q = q(x,t) \in \mathbb{R}^m$ is the vector of conserved quantities, $f(q)$ is the flux function which depends explicitly on x and t as well as on q, ψ is the source term, which can be used for geometric sources of the conserved quantities, reaction or

viscous effects, κ is the capacity function, which represents the accumulation of the conserved quantities in the problem domain.

In the standard (linear, data-independent) conservative case, $\kappa \equiv 1$ and $\psi \equiv 0$, therefore

$$q_t + f(q)_x = 0 \tag{4.18}$$

The CLAWPACK's approach to solving hyperbolic conservation laws relies on the Riemann solution. The numerical techniques utilized in the software, such as finite volume methods, necessitate a Riemann solver to capture wave propagation accurately. The "Riemann solver" refers to a numerical approach for converting the discontinuity at the interface of two grid cells into waves that propagate to adjacent cells.

The flux function $f(q)$ can also depend explicitly on x and t as well as on q. Hyperbolic systems that are not in conservative form can also be solved:

$$q_t + \mathfrak{B}(x,t)q_x = \mathcal{S} \tag{4.19}$$

A Riemann solver to be specified for any two states q_{i-1} and q_i should return a set of waves $\mathcal{W}^p$ satisfying

$$\sum_{p=1}^{M_w} \mathcal{W}_i^p = q_i - q_{i-1} \equiv \Delta q_i. \tag{4.20}$$

$\mathcal{W}^p$ is the jump in q across the p^{th} wave, M_w is the number of waves, and each wave has an associated wave speed λ^p.

The Riemann solver should provide left and right-going fluctuations, respectively, $\mathfrak{B}^{-}\Delta q_i$ and $\mathfrak{B}^{+}\Delta q_i$. For the standard conservative case, the fluctuations should satisfy:

$$\mathfrak{B}^{-}\Delta q_i + \mathfrak{B}^{+}\Delta q_i = f(q_i) - f(q_{i-1}) \tag{4.21}$$

Then, the fluctuations define a "flux-difference splitting":

$$\mathfrak{B}^{-}\Delta q_i = \sum_p (\lambda_i^p)^{-} \mathcal{W}_i^p \ , \qquad \mathfrak{B}^{+}\Delta q_i = \sum_p (\lambda_i^p)^{+} \mathcal{W}_i^p \tag{4.22}$$

where $\lambda^{-} = \min(\lambda, 0)$ and $\lambda^{+} = \max(\lambda, 0)$.

When employing the first-order Godunov method that utilizes only the fluctuations, it calculates the updated states of the conserved quantities in a specific format.

$$q_i^{n+1} = q_i^n - \frac{\Delta t}{\Delta x}[\mathfrak{B}^{+}\Delta q_i + \mathfrak{B}^{-}\Delta q_{i+1}] \tag{4.23}$$

In order to obtain high-resolution, CLAWPACK's method extends by introducing an additional term. This extension of the technique is in the following form:

$$q_i^{n+1} = q_i^n - \frac{\Delta t}{\Delta x}[\mathfrak{B}^{+}\Delta q_i + \mathfrak{B}^{-}\Delta q_{i+1}] - \frac{\Delta t}{\Delta x}[F_{i+1} - F_i] \tag{4.24}$$

where,

$$F_i = \frac{1}{2}\sum_{p=1}^{M_w} |\lambda_i^p| \left(1 - \frac{\Delta t}{\Delta x}|\lambda_i^p|\right) \mathcal{W}_i^p \tag{4.25}$$

The solution of the Riemann problem is associated with the characteristics of the system equation (i.e. the eigenvector of the coefficient matrix B of the Eqn (4.15)). The eigenvalues of the matrix B are:

$$\lambda^1 = (v - c) \qquad \lambda^2 = (v + c) \tag{4.26}$$

which represent the speed of right-going and left-going waves. However, the eigenvectors are different for each form of the matrix. For the main variables of p and m in Eqns (4.7) and (4.8) the corresponding eigenvectors are:

$$r^1 = \begin{bmatrix} -c \\ (1 - v/c)A \end{bmatrix} \quad r^2 = \begin{bmatrix} c \\ (1 + v/c)A \end{bmatrix} \tag{4.27}$$

A computer model developed by Falk and Gudmundsson for solving mass and momentum equations described in Eqns (4.11) and (4.12) is used to model two-phase homogeneous pressure propagation in pipeline. The system domain is divided into grids and properties of gas and water are defined for the grids. To observe the effect of void fraction, various numbers of gas and water grids are selected. After model construction, a shallow pressure signal (~1bar difference) is sent from the left boundary of the pipe filled with fluid and the method described in Sec (4.1.2) is used to calculate the pressure wave propagation velocity.

4.3.3 2-D Modeling

In this thesis, a mapped grid approach derived from the CLAWPACK software package, as developed by Shyue (2010), is employed to model two-dimensional compressible multiphase flow. This method provides a robust and efficient framework for simulating the complex interactions between different phases within a compressible fluid system. The utilization of CLAWPACK, recognized for its proficiency in solving hyperbolic partial differential equations, ensures the accuracy and reliability of simulations.

The Eulerian viewpoint in fluid dynamics refers to an approach in which the observer's reference frame is fixed in space, and the focus is on studying the flow of fluids at specific points in that space. In the context of the governing equations, such as the Navier-Stokes equations that describe fluid motion, the Eulerian formulation involves expressing the equations in terms of fixed spatial coordinates, often Cartesian coordinates. The principal motion of each phase is described as:

$$\frac{\partial}{\partial t}\begin{pmatrix} \rho \\ \rho u_i \\ E \end{pmatrix} + \sum_{j=1}^{N_d} \frac{\partial}{\partial x_j}\begin{pmatrix} \rho u_j \\ \rho u_i u_j + p\delta_{ij} \\ E u_j + p u_j \end{pmatrix} = 0 \tag{4.28}$$

where N_d is the number of spatial dimensions and $i = 1,2, \dots, N_d$. The properties ρ, u_j, p, E and δ_{ij} are density and particle velocity in the x_j-direction, pressure, total energy, and the Kronecker delta, respectively. The total energy is defined as:

$$E = \rho e + \sum_{j=1}^{N_d} \frac{\rho {u_j}^2}{2} \tag{4.29}$$

As proposed by Shyue (2010), the linearized Mie-Grüneisen equation of state (EOS) is a model used to describe the thermodynamic behavior of materials, particularly in the context of high-pressure and shockwave physics. This particular equation of state combines the principles of the stiffened gas model with a linear dependence on density, offering a simplified yet practical approach for analytical and computational analyses.

$$p(\rho, e) = (\gamma - 1)\rho e + (\rho - \rho_0)c^2 \tag{4.30}$$

where e is the internal energy, γ is the specific heat ratio, ρ_0 is the reference values of density and c is the speed of sound.

In order to properly model the front tracking of the pressure wave propagation in a flow with complex geometries, a mapped grid method is used. The core governing equations in the mapped grid algorithm comprise two main components. The Euler equations are applied within a curvilinear coordinate system to model the motion of fluid mixtures, incorporating conserved variables within multiphase grid cells. By implementing mass and energy conservations, a set of effective equations is obtained for material quantities pertinent to the specific problem within these cells. Basically, the aforementioned curvilinear mapping for the two-dimensional physical domain (x_1, x_2) to the computational domain (ξ_1, ξ_2) is described as in:

$$\begin{aligned} dx_1 &= a_1 d\xi_1 + a_2 d\xi_2 \\ dx_2 &= b_1 d\xi_1 + b_2 d\xi_2 \end{aligned} \tag{4.31}$$

where a_i are b_i the metric terms of the mapping.

The numerical solution of the 2-D model relies on solving 1-D Riemann problems at every cell edge. This means that the waves emerging from the problem are utilized to update the average values of the cells neighboring each edge. The 2-D quadrilateral grid, as described in Eqn (4.31), is used in conjunction with a finite volume method to obtain an approximation of the cell average of the solution q over the (i,j)th grid cell at a time t_n. Essentially:

$$Q^n{}_{ij} \approx \frac{1}{M(C_{ij})} \int_{C_{ij}} q(x_1, x_2, t_n) dx_1 dx_2 \tag{4.32}$$

$$= \frac{1}{J(C_{ij})\Delta\xi_1\Delta\xi_2} \int_{\hat{C}_{ij}} q(x_1, x_2, t_n) d\xi_1 d\xi_2$$

where C_{ij} and $\hat{C}_{ij}$ are the regions occupied by the grid cell in physical and computational domains, respectively. $M(C_{ij})$ is the measure area of C_{ij} and $J(C_{ij})$ is the Jacobian of the mapping of the cell.

As in solution of 1-D numerical model, a fully discrete version of the pressure wave propagation method for Godunov-type scheme is offered:

$$Q^{n+1}{}_{ij} = Q^n{}_{ij} - \frac{1}{J(C_{ij})}\frac{\Delta t}{\Delta\xi_1}(A^+{}_1\Delta Q_{i-\frac{1}{2j}} + A^-{}_1\Delta Q_{i+\frac{1}{2j}} \tag{4.33}$$

$$- \frac{1}{J(C_{ij})}\frac{\Delta t}{\Delta\xi_2}(A^+{}_2\Delta Q_{i-\frac{1}{2j}} + A^-{}_2\Delta Q_{i+\frac{1}{2j}}$$

where $A^+{}_1\Delta Q_{i-\frac{1}{2j}}$, $A^-{}_1\Delta Q_{i+\frac{1}{2j}}$, $A^+{}_2\Delta Q_{i-\frac{1}{2j}}$ and $A^-{}_2\Delta Q_{i+\frac{1}{2j}}$ are right, left, up and down moving fluctuations, respectively. The program solves Riemann problem in the x_1, direction, firstly transforming $Q^{n+1}{}_{ij}$ and $Q^n{}_{ij}$ into $\widetilde{Q_R}$ and $\widetilde{Q_L}$.After defining scaled speeds, it determines left, right, up and down moving fluctuations. In this thesis, the detailed working principles of the given program were not explored as it falls beyond the scope of the study.

CHAPTER 5

RESULTS AND DISCUSSION

5.1 Results of Field Measurements

Understanding the dynamics of liquid-gas two-phase flow within a pipeline is crucial, and a critical aspect of it involves characterizing the distribution of the liquid and gas phases. This characterization is evident through commonly observed flow structures known as two-phase flow patterns or flow regimes, each with distinct identifying characteristics. For instance, local pressure drops, heat transfer coefficients, and the propagation of pressure waves through the flowing fluid are closely correlated with the prevailing two-phase flow structure.

In Figure 5.1, the flow regimes encountered in the wells are presented according to two different two-phase gas-liquid horizontal flow regime maps based on the superficial phase velocities ((Mandhane et al., 1974; Taitel & Dukler, 1976)). The observed flow regimes in the field tests include dispersed bubble, elongated bubble, and slug flows. Since the flow regimes are not segregated flow regime types (such as stratified or wavy), the measured propagation speed of pressure waves values should be more reliable and accurate due to presence of some degree of homogenization of phases as the flow takes place along approximately 30 meters horizontal flow line.

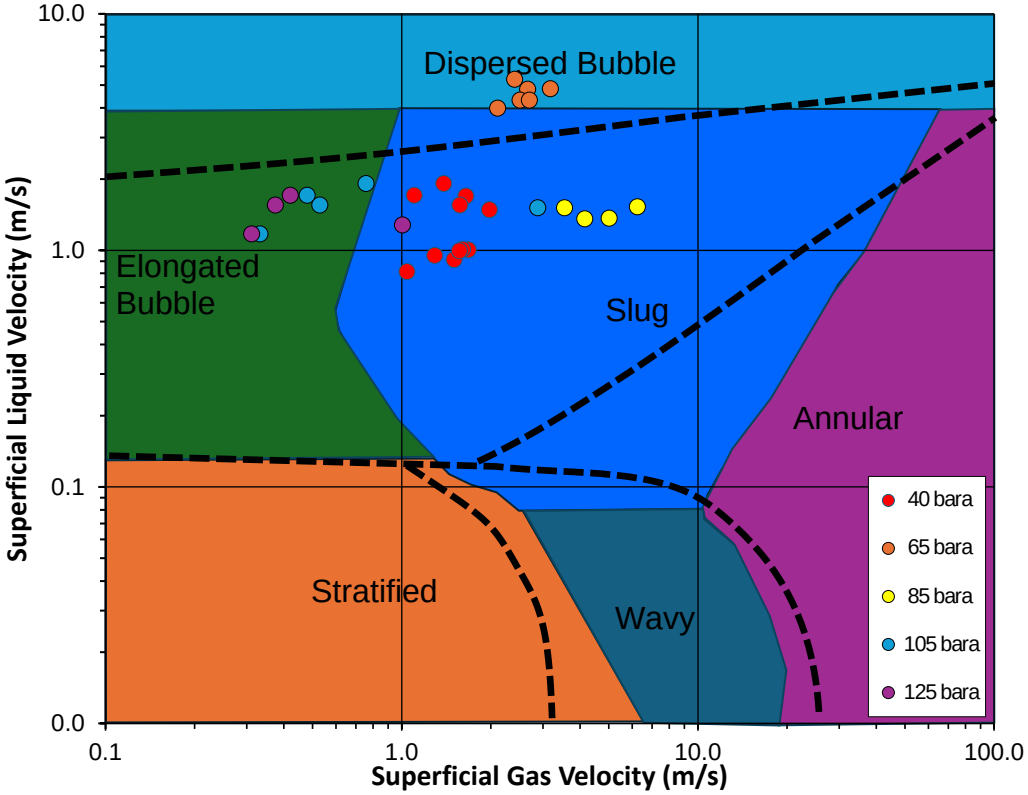

Figure 5.1 Two-phase gas-liquid horizontal flow regimes map of Mandhane et at. (1974) (colored areas) and Taitel and Dukler, (1976) (black dashed lines) and the measured data.

The field data contains pressure measurements, oil/gas gravities (37°API for oil and 1.1-1.25 for gas), separator GOR and water cut values from 4 wells during a test project conducted in Norway. All four producer wells were part of a reservoir undergoing water alternate gas injection (WAG) treatment, wherein the injectors alternatingly changed from gas to water injection at specific intervals. Pressure signals were recorded using the set-up located at the surface. There are two pressure transmitters, one placed after the wellhead and the other upstream of the choke. The distance between two transmitters is given as 30 – 35 m changing for each well.

The estimated propagation speed of pressure waves values from cross-correlation against void fractions are presented in Tables 5.1 to 5.5 for the grouped wellhead

pressure ranges of 40, 65, 85, 105, and 125 bara, respectively. These values were obtained using a shifting time-window approach for each test. Therefore, calculated values were averaged, and their standard deviations were calculated and presented in Appendix B.

The multiphase flow condition along the flowline is analyzed using the steady-state multiphase simulator PIPESIM to evaluate the effect of the slip phenomenon on void fractions. The same flowline segment is simulated using consistent separator data to obtain void fractions, gas, liquid, mean slip velocities. The results are reported in Table A - 2 and Table A - 3, and the void fractions obtained from the multiphase steady-state flow simulations (including the slip effect) are compared with the void fractions obtained under the no-slip assumption (from Eqn. 4.2) in **Figure 5.2**. It is observed that, in the flowing condition (considering the slip effect), the void fraction decreases by an average of 13% (i.e., the slip void fraction is less than the no-slip void fraction). This is expected because the faster movement of the gas phase (due to slip) implies that the actual in-situ gas volume at any specific point in the flowline is less than the volume calculated by homogeneous mixing and the no-slip condition.

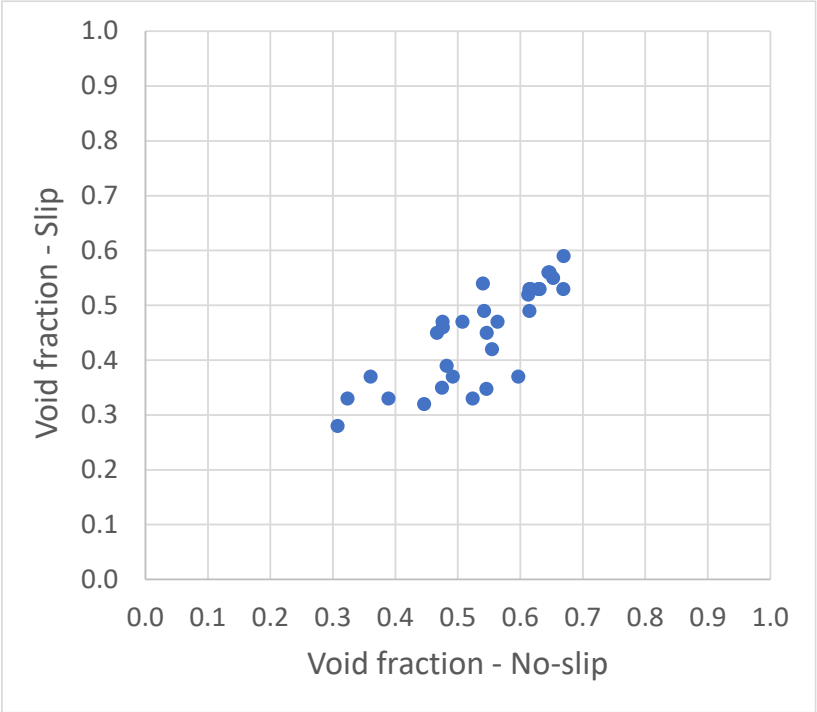

Figure 5.2 Void fraction, slip vs no-slip.

In addition to the measured propagation speed of pressure waves values, two empirical model results (namely Wood and Dong & Gudmundsson models), and the transient multiphase flow model (OLGA) results are presented as graphs plotted against void fractions in Figure 5.3 to Figure 5.7 at the specified pressures and temperatures. The in-situ void fractions for each test data point on the figures are estimated from Eqn (4.11) using the gas gravity and API gravity of oil, separator water cut (WC) and GOR in field data. The test separator results are reported at standard conditions (1 bar and 15 C). The produced oil has an average of 37°API and the average gas specific gravity is 1.17. The salt content of the produced water was 39 ppt. The formation volume factors of each phase at the given pressure and temperature are calculated from the fluid properties and using correlations and PVT models following the methods stated in Dong and Gudmundsson work (1993). The error bars on the figures indicate relative standard deviations of the measured propagation speed of pressure waves values.

Calculation of propagation speed of pressure waves by two empirical models are performed for each pressure range group. The Dong and Gudmundsson model utilized as in Eqn (2.15) with fractions, physical properties, and thermodynamic properties of gas, oil, and water phases. The Wood model utilized as in Eqn (2.8) and fractions, along with physical properties of gas and liquid phases. In these calculations, watercut was taken as the average of watercut values at each pressure range group.

It is clearly seen in the graphs that the speed of sound of pure liquid is high and decreases abruptly with any amount of gas added into liquid. In between void fraction of approximately 0.2 to 0.8, the values remain constant and for pure gas, speed increases sharply. Moreover, the speed of sound in pure liquid is much higher than in pure gas.

Comparing the two empirical model results with field measurements and the transient numerical model estimations, we observed that the Wood model generally overestimates, except for the lowest wellhead pressure data. Conversely, the Dong and Gudmundsson model performed better at predicting sound speed, except for the lowest wellhead pressure data. Measured data aligns more closely with the OLGA results across almost the entire pressure range. Deviations of measured results from the calculated and simulated values might be due to slugging flow behavior in flowline.

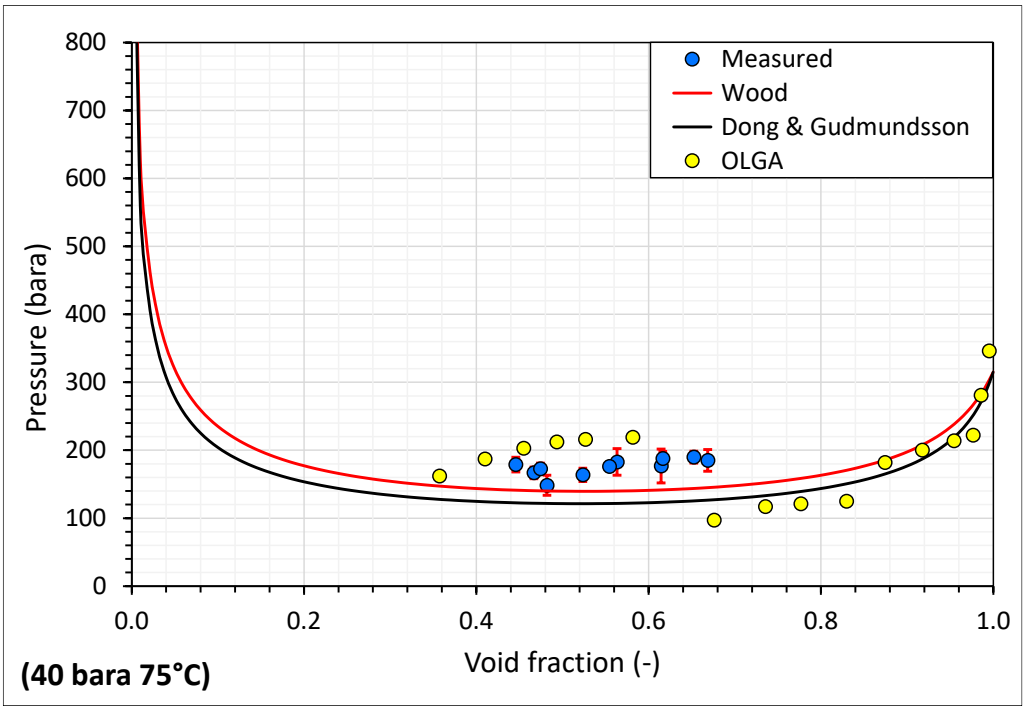

Figure 5.3. Comparison of the measured propagation speed of pressure waves with values obtained from Wood, Dong and Gudmundsson equations and OLGA modelling at 40 bar and 75°C.

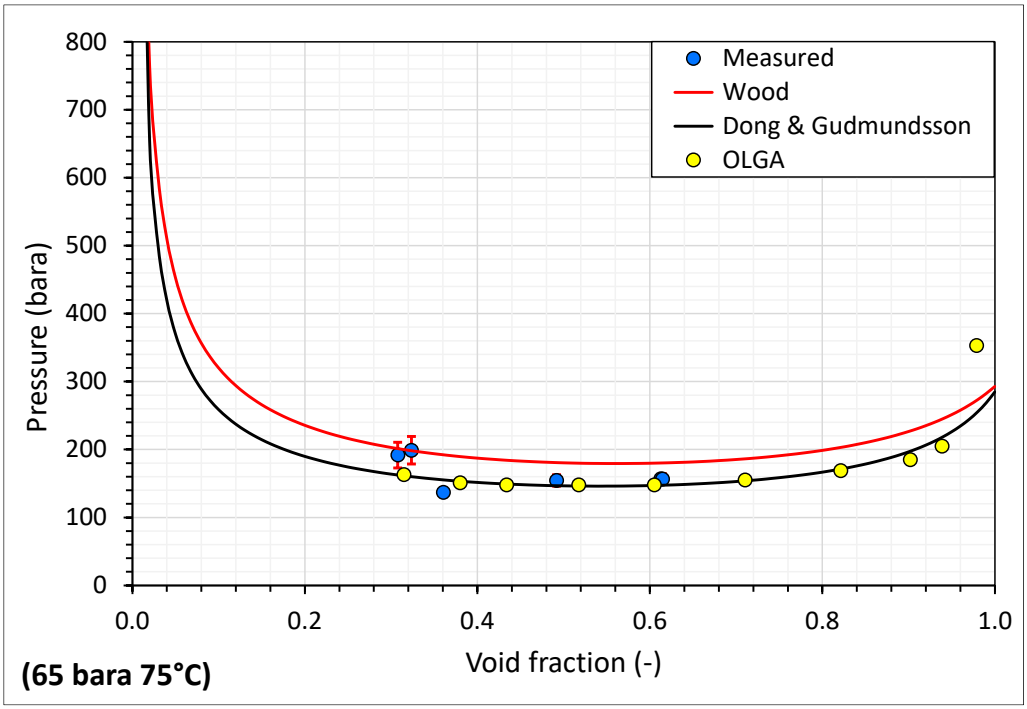

Figure 5.4. Comparison of the measured propagation speed of pressure waves with

values obtained from Wood, Dong and Gudmundsson equations and OLGA modeling at 65 bar and 75°C.

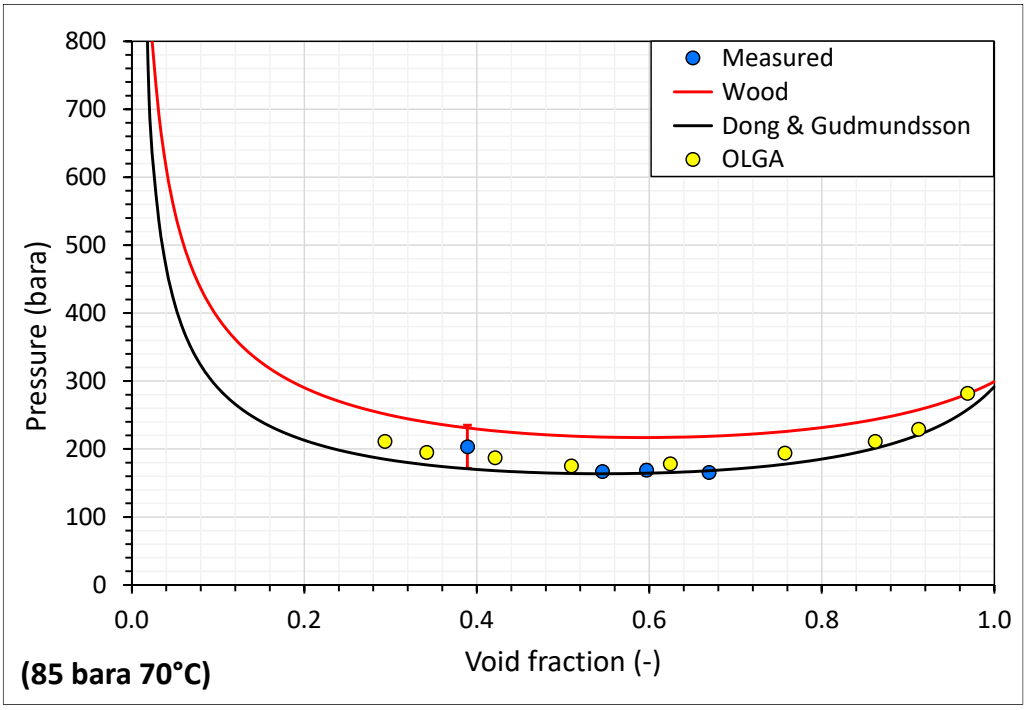

Figure 5.5. Comparison of the measured propagation speed of pressure waves with values obtained from Wood, Dong and Gudmundsson equations and OLGA modelling at 85 bar and 70°C.

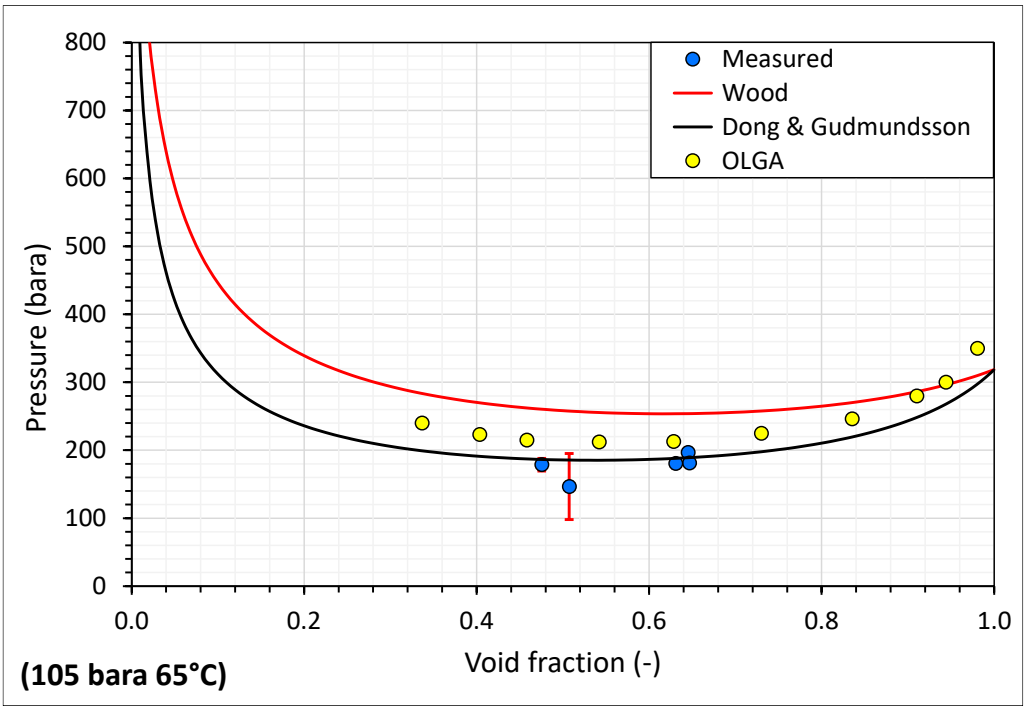

Figure 5.6. Comparison of measured propagation speed of pressure waves with values obtained from Wood, Dong and Gudmundsson equations and OLGA modeling at 105 bar and 65°C.

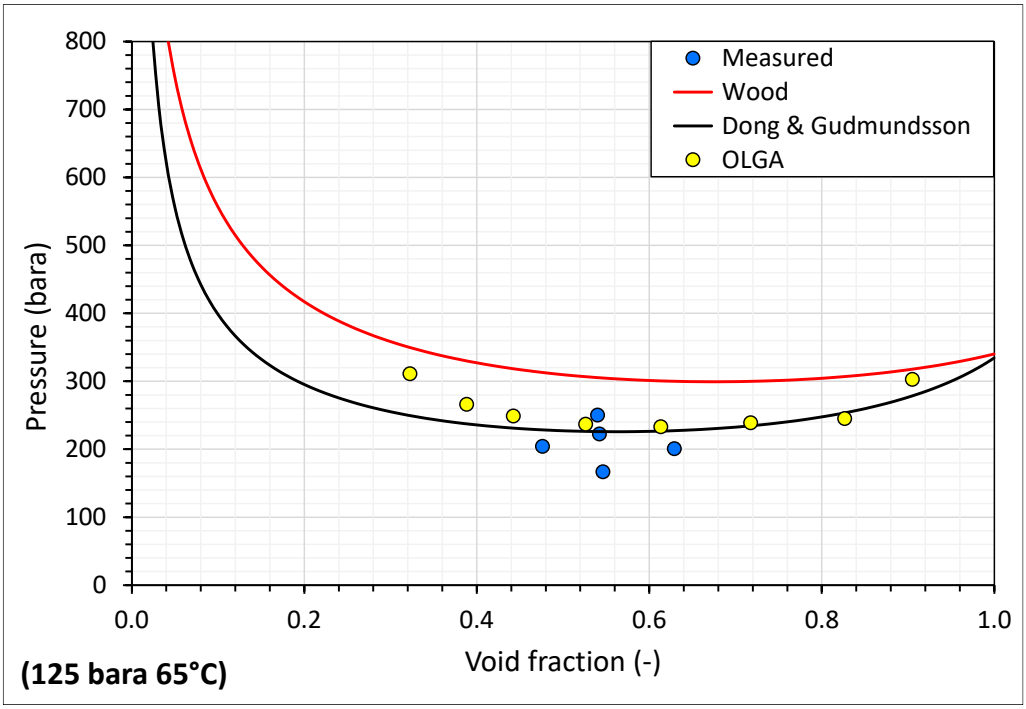

Figure 5.7. Comparison of measured propagation speed of pressure waves with values obtained from Wood, Dong and Gudmundsson equations and OLGA modeling at 125 bar and 65°C.

Upon comparing the outcomes of two empirical models with field measurements and transient numerical model estimations, it was observed that the Wood model generally tends to overestimate, with the exception of the lowest wellhead pressure data. Conversely, the Dong and Gudmundsson model exhibited superior performance in predicting sound speed, with an exception at the lowest wellhead pressure data. Notably, the measured data aligns more closely with the OLGA results across almost the entire pressure range. Discrepancies between the measured results and the calculated and simulated values may be attributed to slugging flow behavior in the flowline.

5.2 Results from 1D Numerical Model

The numeric model, explained in Sec. (4.4) is used and modified for homogeneous multiphase flow. The model domain is divided into 2000 grids and the phases are

defined for the specified number of grids. The input data for the 1D model is given in Table 5-1.

Table 5-1 Input data for 1D numeric model

For water phase	$\rho, kg/m^3$	1000
	$c, m/s$	1500
For gas phase, @ 1bara and 20 C°	$\rho, kg/m^3$	28
	$c, m/s$	436
Pipeline length, m	x	200
Pipeline diameter, mm	d	7.42

The air gun property is used to initiate a pressure wave, which is applied for 0.03 s and an insignificant mass of gas is injected from the left boundary. The simulation is run for 0.5 s and the two pressure measurement points in the pipeline are used to calculate propagation speed of pressure waves from flight time of the wave, located at 10 m and 110 m. In a 200-meter pipeline, 2000 grids were defined, with gas properties assigned to every 60th grid and water properties assigned to every 40th grid. Figure 5.8 gives a small-scale representation of the grid distribution defined initially to the program. Consequently, the void fraction is 0.6 for this example case (Figure 5.9). The propagation speed of pressure wave is measured as 529 m/s.

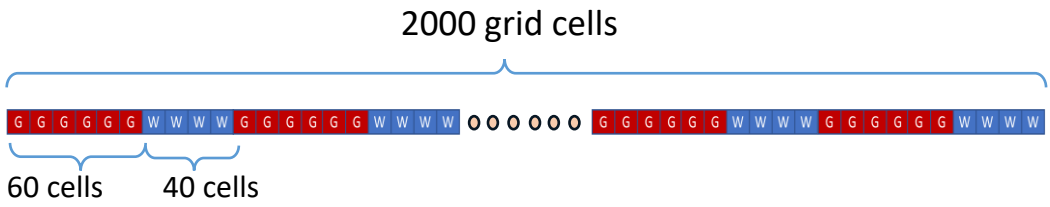

Figure 5.8 Basic schematic of system domain for 1-D model (G=Gas, W=Water)

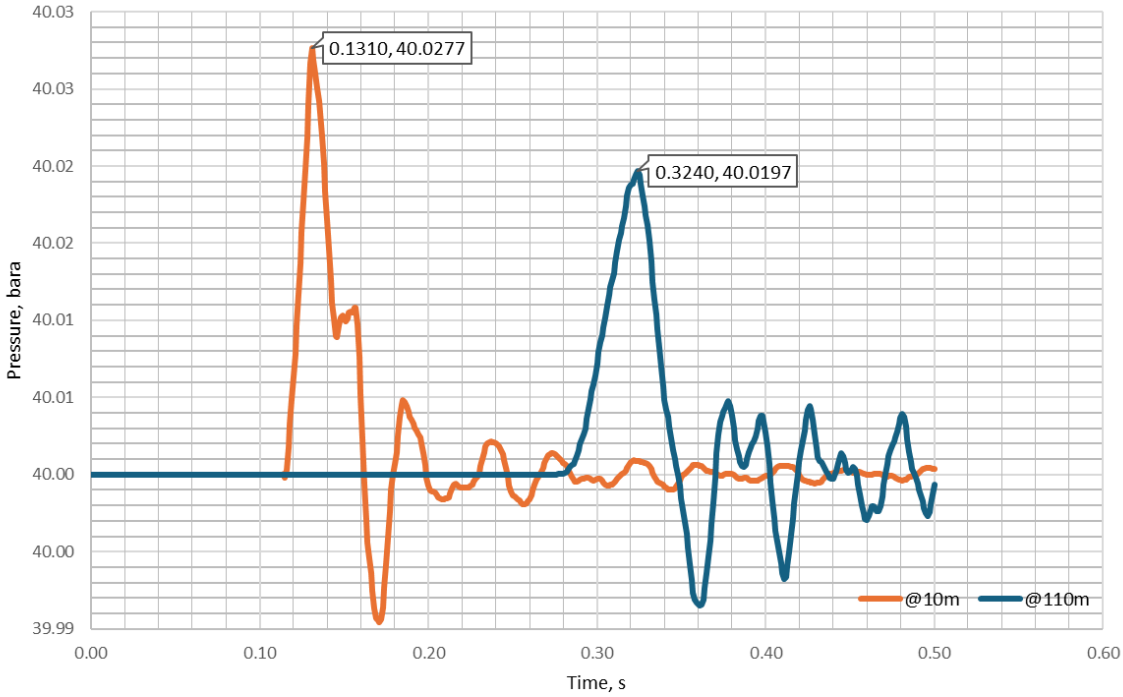

Figure 5.9 Two pressure signals located at 10 m and 110 m

In Table 5-2, the results for 1-D model are provided. Diverse gas and water grid numbers are defined between 3 to 100, and propagation speed of pressure waves s are calculated according to the corresponding void fractions. The plot of propagation speed of pressure waves vs void fraction is given in Figure 5.10. The findings suggest that when encountering a low-density fluid, there is a noticeable decrease in velocity. The calculations are in line with Wood's graph shape, but our study observed higher values, indicating a potentially significant variation from the expected results.

Table 5-2 Propagation speed of pressure waves calculations for different void fractions

nGas	nLiq	Void	Velocity, m/s
3	100	0.03	1370
10	100	0.09	1064
20	100	0.17	833
24	80	0.23	741
24	60	0.29	719
30	60	0.33	662
40	60	0.40	613
50	50	0.50	575
60	40	0.60	529
60	30	0.67	500
60	24	0.71	500
80	24	0.77	490
100	20	0.83	493
100	10	0.91	463
100	3	0.97	446

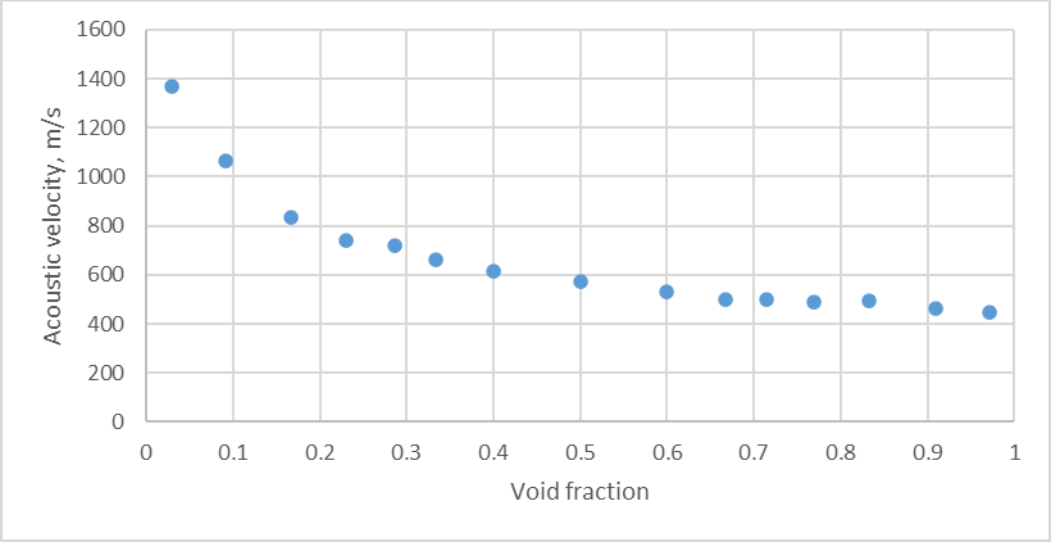

Figure 5.10 Propagation speed of pressure waves vs void fraction plot from 1-D numerical model

5.3 Results from 2D Numerical Model

5.3.1 Model verification

The model needs to be validated using single-phase flow in a pipeline, as the 2D numerical model system is more complex compared to the 1D system. As outlined in Sec. (4.4), the 2D model is based on CLAWPACK software package and modified by Shyue (2010) to model the compressible multiphase flow. The inputs of the model are provided in Table 5-3.

Table 5-3 Input values used to validate the model

For Water	γ	4.4
	$\rho, kg/m^3$	1000
For Air	γ	1.4
	$\rho, kg/m^3$	1.2
Pipeline length, m	x	30
Pipeline diameter, mm	d	120

The model domain is divided into 1000 cells in the x direction and 200 cells in the y direction. Within the pipeline, pressure is measured at three points located at 1.5m, 9m, and 18m. The results from a single water flow are depicted in Figure 5.11. A pressure wave with a 1 bar difference is applied from the left boundary, and the propagation speed of pressure wave of the fluid is determined to be 1496 m/s by calculating the flight time of the created pressure wave, which is close to the speed of sound in water. As in water flow, the same procedure is applied to air flow and the propagation speed of pressure wave is found to be 330 m/s (Figure 5.12).

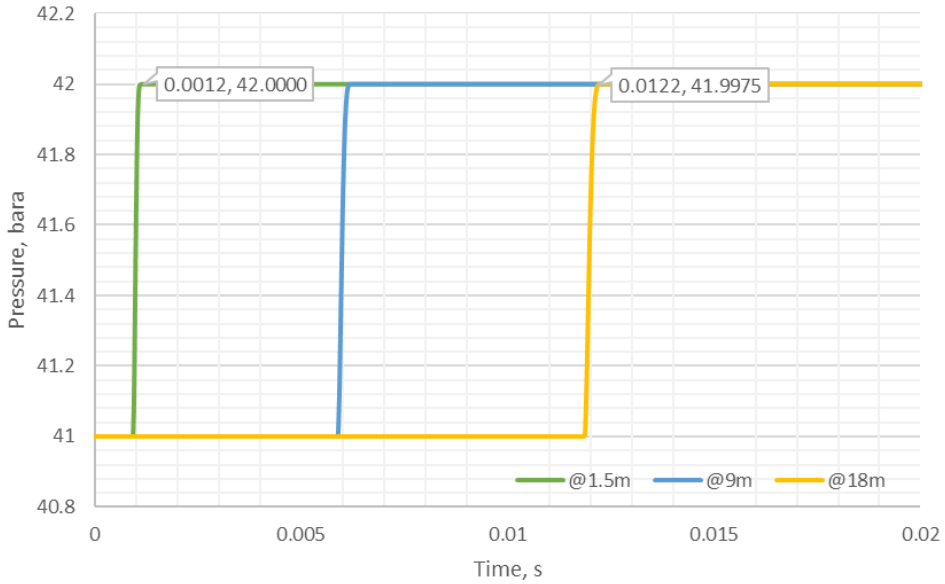

Figure 5.11 Pressure vs. time plot of water flow in pipeline by 2D model.

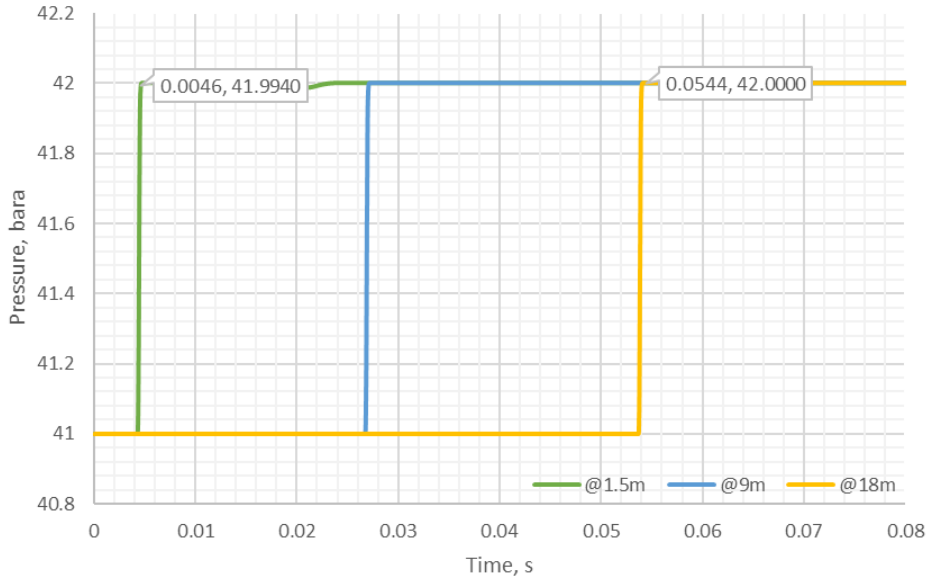

Figure 5.12 Pressure vs. time plot of air flow in pipeline by 2D model.

The model was validated upon completion, and subsequent studies will be conducted based on this validation.

5.3.2 Pressure Wave Propagation in Dispersed Flow Case

The horizontal flow of dispersed flow is simulated using the numerical model introduced Shyue (2010). The bubbles are located at the entrance of $x_1 = 1$ flowline and as an initial condition, a rightward-going shock wave with Mach of 1.422 is given. Although, this case is an extreme case for this study, the effect of higher pressure initiation is monitored. In Figure 5.13, density and pressure graphs are shown at different times $t = 0, 0.3, 0.5, 1.2, 1.6$ and 2.5 ms. These graphs provide insights into the evolution of density and pressure over time, offering a visual representation of the dynamic behavior of the bubble flow in the horizontal flow line. While the shock wave pressure advances through the system, the shape of the bubbles changes because of the high pressure, and gas density increases. 10^9

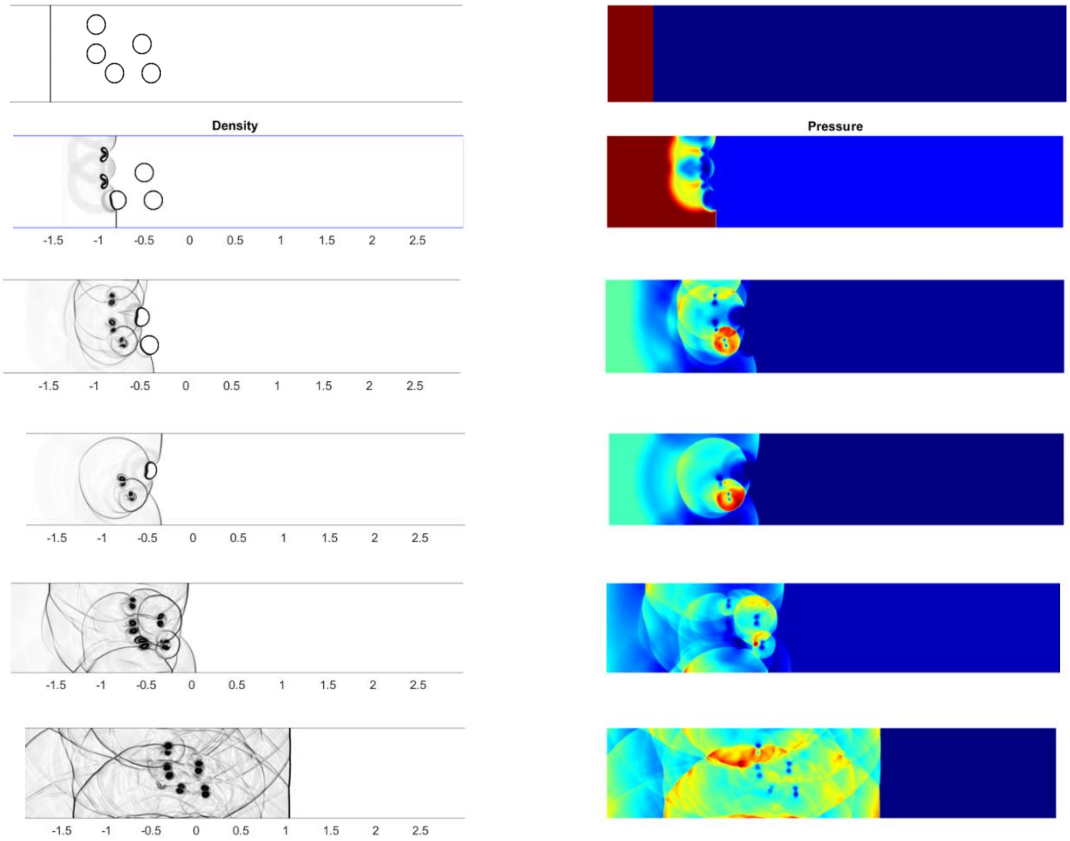

Figure 5.13 Density (left) and pressure (right) graphs for shock wave propagation case for t=0,0.3,0.5,1.2,1.6 and 2.5 ms, respectively

In the given scenario, a relatively lower pressure boundary is applied from the left of the system. In this case, 4 bubbles with larger diameters are identified, and the properties of the pipeline and the phases are provided in Table 5-3. The pressure inside the pipeline is 40 bara, with a 50 bara pressure present on the left. The pressure propagation can be observed in Figure 5.14. Due to the lower pressure difference, the density of the gas phase remains relatively constant, but the effects of the pressure wave are noticeable on the right side of the figure. When compared to the previous case, there is no formation of a shock front by the pressure wave, but the effect of the wave diminishes upon encounter with a lower-density medium.

Although the wave propagation studied in the 2-D model, the calculation of propagation speed of pressure waves cannot be achieved due to the complexity of the model.

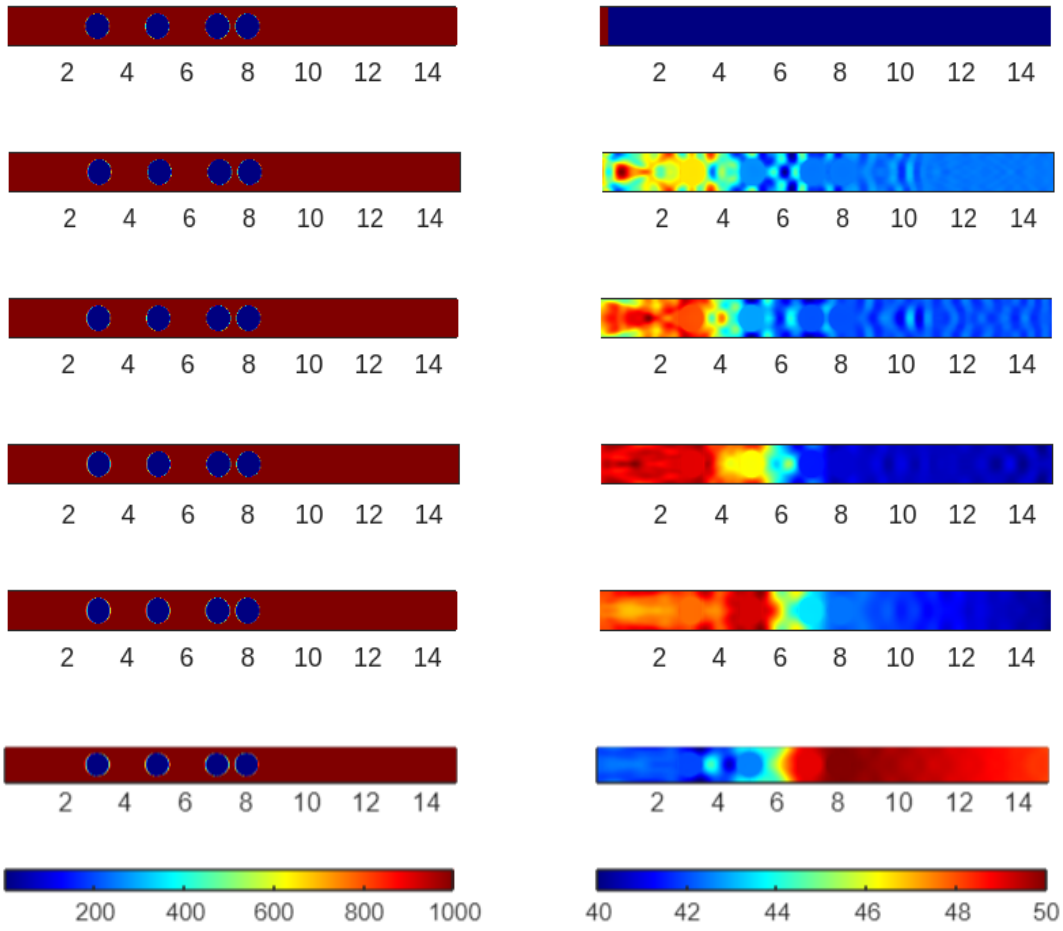

Figure 5.14 Density (left) and pressure (right) graphs for lower pressure boundary case for t=0, 0,01, 0.02, 0.03, 0.05 and 0.07 ms, respectively

CHAPTER 6

CONCLUSION

The objective of this study is to utilize a comprehensive model for gas-liquid flow in oil production pipelines, with a specific focus on calculating the propagation speed of pressure waves within the mixture. By leveraging data collected from a North Sea offshore production platform, the research developed a method to determine the speed of pressure waves, offering valuable insights into fluid dynamics that are crucial for optimizing pipeline operations in the oil and gas industry.

The modeling process includes analyzing diverse flow regimes to capture the complex dynamics of multiphase flow. A pressure wave is introduced to simulate real-world conditions, allowing for the calculation of the propagation speed of pressure waves within the mixture. The numerical solution is used through the demanding application of the finite volume method to the Riemann problem.

In the course of this investigation, the propagation speed of pressure waves within a multiphase fluid is determined by employing the cross-correlation technique on two pressure signals derived from natural disturbances within a pipeline. The outcomes of this method demonstrate a notable correspondence when benchmarked against a prescribed mathematical model, particularly under conditions of elevated pressure. Our investigations revealed several important findings. The Wood model tends to overestimate the propagation speed of pressure waves, particularly its overestimation, which increases with increasing pressure. On the other hand, the Dong and Gudmundsson model is better predicted than the Wood model. Furthermore, the results from OLGA program consistently matches the measured data for almost the entire pressure range.

The study provides empirical validation, establishing that the estimation of the propagation speed of pressure waves through the cross-correlation of pressure data obtained from two distinct points along a pipeline—predicated on the time delay between these signals—proves to be both effective and straightforward. Notably, this method is deemed suitable for on-site applications, showcasing its practical utility in real-world scenarios for multiphase flows, particularly at pressures exceeding the 40-bar threshold. The findings underscore the viability of the cross-correlation approach as a reliable and accessible means for estimating the propagation speed of pressure waves in high-pressure multiphase fluid systems.

The 1-D and 2-D numerical models show the effects on the pressure wave created in a pipeline. The results indicated that the speed of sound affects the amplitude of a pulse, especially when the velocity changes gradually or encounters a discontinuity. When a pulse moves from a low-speed region to a high-speed region, it results in a transmitted pulse with higher pressure. Although the effects can be detected in 2-D model, the calculation of the propagation speed of pressure waves as in 1-D model could not be possible due to the complexity of the model. As a recommendation, further analyses of the equation of the state given and the boundary condition applied should be studied in detail.

REFERENCES

Al-Kadem, M., Gomaa, M., Yateem, K. Al, & Maghlouth, A. Al. (2022). Multiphase Flowmeter Health Monitoring Strategy: Maximizing the Value of Real-Time Sensors and Automation for Industrial Revolution 4.0. *SPE Production & Operations*, *37*(03), 533–542. https://doi.org/10.2118/206281-PA

Al-Kadem, M. S., Al Khelaiwi, F. T., Al Mashhad, A. S., & Al Dabbous, M. S. (2014). A decade of experience with multiphase flow meters. *Society of Petroleum Engineers - International Petroleum Technology Conference 2014, IPTC 2014 - Innovation and Collaboration: Keys to Affordable Energy*, *5*, 3824–3835. https://doi.org/10.2523/IPTC-18162-MS

Al-Safran, E. M., & Brill, J. P. (2017). Applied Multiphase Flow in Pipes and Flow Assurance: Oil and Gas Production. *Applied Multiphase Flow in Pipes and Flow Assurance: Oil and Gas Production*. https://doi.org/10.2118/9781613994924

Barbosa, P. R., Crivelaro, K. C. O., & Seleghim, P. (2010). On the application of self-organizing neural networks in gas-liquid and gas-solid flow regime identification. *Journal of Brazilian Society of Mechanical Sciences and Engineering*, *32*(1), 15–20. https://doi.org/10.1590/S1678-58782010000100003

Barnea, D., Shoham, O., Taitel, Y., & Dukler, A. E. (1980). Flow pattern transition for gas-liquid flow in horizontal and inclined pipes. Comparison of experimental data with theory. *International Journal of Multiphase Flow*, *6*(3), 217–225. https://doi.org/10.1016/0301-9322(80)90012-9

Beggs, D.H., U.; Brill, J.P., U. (1973). A Study of Two-Phase Flow in Inclined Pipes. In *Journal of Petroleum Technology* (Vol. 25, Issue 5, pp. 607–617). https://doi.org/10.2118/4007-PA

Bendlksen, K. H., Malnes, D., Moe, R., & Nuland, S. (1991). The dynamic two-fluid model OLGA; Theory and application. *SPE (Society of Petroleum Engineers) Production Engineering; (United States)*, *6:2*(2), 171–180. https://doi.org/10.2118/19451-PA

Brustur, A.-G. (2014). Multiphase flow in pipelines: An analysis of the influence of empirical correlations on mechanistic models.[Doctoral Dissertation]. *Curtin University. Department of Chemical Engineering*

Chisholm, D. (1967). A theoretical basis for the Lockhart-Martinelli correlation for two-phase flow. *International Journal of Heat and Mass Transfer*, *10*(12), 1767–1778. https://doi.org/10.1016/0017-9310(67)90047-6

Crawford, T. J., Weinberger, C. B., & Weisman, J. (1985). Two-phase flow patterns and void fractions in downward flow Part I: Steady-state flow patterns. *International Journal of Multiphase Flow*, *11*(6), 761–782. https://doi.org/10.1016/0301-9322(85)90023-0

Dong, L., & Gudmundsson, J. S. (1993a). Model for Speed of Sound In Multiphase Mixtures. *3rd Lerkendal Petroleum Engineering Workshop*.

Dong, L., & Gudmundsson, J. S. (1993b). Model for Speed of Sound In Multiphase Mixtures. *3rd Lerkendal Petroleum Engineering Workshop*.

Durran, D. R. (1999). Numerical Methods for Wave Equations in Geophysical Fluid Dynamics . New York (N.Y.) : Springer, 1999. ISBN: 0387983767

Engelbrecht, J. (1997). Nonlinear Wave Dynamics: Complexity and Simplicity. *Springer Netherlands.* ISBN 9048148332

Falk, K. (1999). Pressure Pulse Propagation in Gas-Liquid Pipe Flow: Modeling, Experiments, and Field Testing. *Norwegian University of Science and Technology*.

Ferro, S. P., & Goldschmit, M. B. (2007). A Numerical Model for Multiphase Flow on Oil Production Wells. *Proceedings of the SPE Latin American and Caribbean Petroleum Engineering Conference*, *2*, 1037–1042. https://doi.org/10.2118/107771-MS

Fu, K., Deng, X., Jiang, L., & Wang, P. (2020). Direct numerical study of speed of sound in dispersed air–water two-phase flow. *Wave Motion*, *98*. https://doi.org/10.1016/J.WAVEMOTI.2020.102616

Godunov, S. K. (1959). A difference method for numerical calculation of discontinuous solutions of the equations of hydrodynamics. *Matematicheskii Sbornik*. 47, 271-306. (Vol. 89, Issue 3).

Graham, E., Castillo, L., Yi, J., Mooney, T., Jadot, T., & Amin, A. (2022). Subsea Multiphase Flow Meter Measurement Performance Assurance with an Applied Data Validation and Reconciliation Surveillance Methodology. *Proceedings of the Annual Offshore Technology Conference*. https://doi.org/10.4043/31836-MS

Gudmundsson, J. S. (1998). US Patent for Method for Determination of Flow Rate in a Fluid. Patent number: 5741978.

Guo, B., Song, S., Ghalambor, A., & Lin, T. R. (2014). Offshore pipelines: Design, installation, and maintenance. Elsevier Science. ISBN: 9780123984920

Guo, X., Deng, J., & Cao, Z. (2022). Study on the Propagation Characteristics of Pressure Wave Generated by Mechanical Shock in Leaking Pipelines. *Chemical Engineering Research & Design*, *164*, 706–714. https://doi.org/10.1016/J.PSEP.2022.06.038

Hagedorn, A. R., & Brown, K. E. (1965). Experimental Study of Pressure Gradients Occurring During Continuous Two-Phase Flow in Small-Diameter Vertical Conduits. *Journal of Petroleum Technology*, *17*(04), 475–484. https://doi.org/10.2118/940-PA

Hanafizadeh, P., Hojati, A., & Karimi, A. (2015). Experimental investigation of oil–water two phase flow regime in an inclined pipe. *Journal of Petroleum Science and Engineering*, *136*, 12–22. https://doi.org/10.1016/J.PETROL.2015.10.031

Hanson, D., Randall, R. B., Brown, G., & Emslie, R. (2008). Locating leaks in underground water pipes using the complex cepstrum. *Australian Journal of Mechanical Engineering*, *6*(2), 107–112. https://doi.org/10.1080/14484846.2008.11464564

Henry, R. E. Gromler, M.A., Fauske, H. A. (1971). Pressure Pulse Propagation in Two Phase One and Two Component Mixtures. *Argonne National Laboratory, March 1971*.

Hewitt, G. F., & Roberts, D. N. (1969). Studies of two-phase flow patterns by simultaneous x-ray and flast photography. [Technical Report]. United Kingdom.

Hibiki, T., & Ishii, M. (2003). One-dimensional drift-flux model and constitutive equations for relative motion between phases in various two-phase flow regimes. *International Journal of Heat and Mass Transfer*, *46*(25), 4935–4948. https://doi.org/10.1016/S0017-9310(03)00322-3

Kieffer, S. W. (1977). Sound Speed in Liquid-Gas Mixtures Water-Air and Water-Steam. *Journal of Geophysical Research*, *82*(20), 2895–2904. https://doi.org/10.1029/JB082i020p02895

Kozubkova, M., Jablonska, J., Bojko, M., Dvorak, L., & Carnogurska, M. (2019). Multiphase fluid models to deal with fluid flow dynamics. *MM Science*

Journal, *2019*(2), 2891–2896. https://doi.org/10.17973/MMSJ.2019_06_201880

Lee, A.H., & Jepson, W.P. (1993). *Study of Flow Regime Transitions of Oil-Water-Gas Mixtures in Horizontal Pipelines*. *6*(11).

Lee, B. I., & Kesler, M. G. (1975). A generalized thermodynamic correlation based on three-parameter corresponding states. *AIChE Journal*, *21*(3), 510–527. https://doi.org/10.1002/AIC.690210313

LeVeque, R. J. (1992). Numerical Methods for Conservation Laws. *Numerical Methods for Conservation Laws*. https://doi.org/10.1007/978-3-0348-8629-1

LeVeque, R. J. (1995). *CLAWPACK User Notes*. University of Washington. http://www.amath.wasingthon.edu/~rjl/clawpack.html

LeVeque, R. J. (1997). Wave Propagation Algorithms for Multidimensional Hyperbolic Systems. *Journal of Computational Physics*, *131*(2), 327–353. https://doi.org/10.1006/JCPH.1996.5603

Leveque, R. J. (2006). *CLAWPACK Version 4.3 User's Guide*. http://www.amath.washington.edu/~claw/

Lighthill, J. (1978). *Waves in Fluids*. Cambridge University Press.

Li, X., Xue, Y., Li, Y., & Feng, Q. (2023). Computational Fluid Dynamic Simulation of Leakage Acoustic Waves Propagation Model for Gas Pipelines. *Energies*, *16*(2), 615–615. https://doi.org/10.3390/EN16020615

Li, Y., Li, C., Chen, E., & Ying, Y. (2011). Pressure wave propagation characteristics in a two-phase flow pipeline for liquid-propellant rocket. *Aerospace Science and Technology*, *15*(6), 453–464. https://doi.org/10.1016/J.AST.2010.09.011

Lockhart, R. W. , M. R. C. (1949). Proposed Correlation of Data for Isothermal Two-Phase, Two-Component Flow in Pipes. *Chemical Engineering Progress*.

Mandhane, J. M., Gregory, G. A., & Aziz, K. (1974). A flow pattern map for gas—liquid flow in horizontal pipes. *International Journal of Multiphase Flow*, *1*(4), 537–553. https://doi.org/10.1016/0301-9322(74)90006-8

Michaelides, E. E. (1981). Thermodynamic Properties of Geothermal Fluids. *Geothermal Resources Council Transactions*, 361–364.

Neogi, S., Lee, A., & Jepson, W. P. (1994). A Model for Multiphase (Gas-Water-Oil) Stratified Flow in Horizontal Pipelines. *SPE - Asia Pacific Oil & Gas Conference*, 553–562. https://doi.org/10.2118/28799-MS

Nguyen, D. L., Winter, E. R. F., & Greiner, M. (1981). Sonic velocity in two-phase systems. *International Journal of Multiphase Flow*, *7*(3), 311–320. https://doi.org/10.1016/0301-9322(81)90024-0

Noble C. A. (2018). Experimental Investigation of Two-Phase (Gas/Liquid) Flow in Intermediate Sized, Horizontal and Inclined Pipes, [Doctoral Dissertation] *University of South Carolina*.

Parlaktuna, M., & Gudmundsson, J. S. (1991). *Physical Properties of Natural Gases: Computer Program and Subroutines*. The Norwegian Institute of Technology.

Retnanto, A., & Azim, A. (2001). *Monitoring Well Performance using Multiphase Flow Meter*. https://doi.org/10.2118/68718-MS

Roe, P. L. (1981). Approximate Riemann solvers, parameter vectors, and difference schemes. *Journal of Computational Physics*, *43*(2), 357–372. https://doi.org/10.1016/0021-9991(81)90128-5

Romate, J. E. (1998). An approximate Riemann solver for a two-phase flow model with numerically given slip relation. *Computers & Fluids*, *27*(4), 455–477. https://doi.org/10.1016/S0045-7930(97)00067-4

Rosa, E. S., Flora, B. F., & Souza, M. A. S. F. (2012). Design and performance prediction of an impedance void meter applied to the petroleum industry. *Measurement Science and Technology*, *23*(5), 055304. https://doi.org/10.1088/0957-0233/23/5/055304

Rowe, A. M., & Chou, J. C. S. (1970). Pressure-Volume-Temperature-Concentration Relation of Aqueous NaCI Solutions. *Journal of Chemical and Engineering Data*, *15*(1), 61–66. https://doi.org/10.1021/JE60044A016/ASSET/JE60044A016.FP.PNG_V03

Russell, D. A. (2013, March). *Reflection of Waves from Boundaries*. https://www.acs.psu.edu/drussell/Demos/reflect/reflect.html

Schlumberger. (2019). *OLGA Dynamic Multiphase Flow Simulator User Manual*.

Shyue, K.-M. (2010). *A high-resolution mapped grid algorithm for compressible multiphase flow problems*.

Taitel Y., & Dukler A. E. (1976). A model for predicting flow regime transitions in horizontal and near horizontal gas-liquid flow. *AIChE Journal*, *22*(1), 47–55. https://doi.org/10.1002/AIC.690220105

Thome J. R. (2004). *Void Fractions in Two-Phase Flows:*The Heat Transfer Engineering Data Book III, *PP Publico Publications*. ISBN -10 3-934736-37-8

Ünalmis, Ö. H. (2016). Sound speed in downhole flow measurement. *The Journal of the Acoustical Society of America*, *140*(1), 430–441. https://doi.org/10.1121/1.4955302

Usov, E. V., Ulyanov, V. N., Butov, A. A., Chuhno, V. I., & Lyhin, P. A. (2020). Modelling Multiphase Flows of Hydrocarbons in Gas-Condensate and Oil Wells. *Mathematical Models and Computer Simulations*, *12*(6), 1005–1013. https://doi.org/10.1134/S2070048220060162

Wallis, G. B. (1969). *One-dimensional two-phase flow, Graham B. Wallis, McGraw-Huill, New York(1969). 18*(6), 431.

Wang, Q., Polansky, J., Karki, B., Wang, M., Wei, K., Qiu, C., Kenbar, A., & Millington, D. (2016). Experimental tomographic methods for analysing flow dynamics of gas-oil-water flows in horizontal pipeline. *Journal of Hydrodynamics, Ser. B*, *28*(6), 1018–1021. https://doi.org/10.1016/S1001-6058(16)60704-7

White, F. M. (1986). *Fluid Mechanics*. McGraw-Hill.

Williams, J. (1994). *SPE 28515 Status of Multiphase Flow Measurement Research*. http://onepetro.org/SPEATCE/proceedings-pdf/94SPE/All-94SPE/SPE-28515-MS/3149046/spe-28515-ms.pdf/1

Wood, A. B. (1955). *Textbook of Sound: Being an Account of the Physics of Vibrations with Special Reference to Recent Theoretical and Technical Developments*. G. Bell and Sons Ltd.

Yadigaroglu, G., Hewitt, G. F., & Banerjee, S. (2018). *Introduction to Multiphase Flow Basic Concepts, Applications and Modelling Zurich Lectures on Multiphase Flow Series Editors*. Springer International Publishing. https://doi.org/DOI 10.1007/978-3-319-58718-9

Zhou, J., & Adewumi, M. A. (1996). Simulation of transients in natural gas pipelines. *SPE Production and Facilities*, 11(4), 202-207. https://doi.org/10.2118/31024-pa

APPENDICES

A. Field Measurements

Production flow rates of each phase measured through the three-phase test separator. The four wells were tested during testing campaign conducted on an offshore production platform.

Table A - 1 The production test data from the test separator.

Well / Test No	WHP bara	WHT °C	Qo Sm^3/d	Qg Sm^3/d	Qw Sm^3/d	Total liq. Sm^3/d	GOR Sm^3/Sm^3	WC (-)
W-1/1	34.1	68.9	447	48461	463	910	108.4	0.51
W-1/2	34.1	71.6	502	53456	499	1001	106.5	0.50
W-1/3	34.6	70.7	463	52276	542	1005	112.9	0.54
W-1/4	35.1	71.5	494	51618	497	991	104.5	0.50
W-1/5	35.9	69.4	464	44149	483	947	95.1	0.51
W-1/6	36.5	76.1	534	55623	1154	1688	104.2	0.68
W-1/7	37.5	67.5	416	37721	394	810	90.7	0.49
W-2/1	52.3	83.2	453	132522	4325	4778	292.5	0.91
W-2/2	55.5	82.7	510	170252	4294	4804	333.8	0.89
W-2/3	63.7	82.1	447	134239	3530	3977	300.3	0.89
W-2/4	82.7	81.4	632	322383	3930	4562	510.1	0.86
W-2/5	104.4	77.6	790	627460	2964	3754	794.3	0.79
W-2/6	122.0	69.9	284	161085	992	1276	567.0	0.78
W-3/1	68.9	60.8	1332	203886	110	1442	153.1	0.08
W-3/2	75.8	60.6	1332	223736	57	1389	168.0	0.04
W-3/3	84.1	60.6	1413	259843	67	1480	183.9	0.05
W-3/4	89.3	58.6	1118	301635	13	1131	269.8	0.01

Well / Test No	WHP bara	WHT °C	Qo Sm^3/d	Qg Sm^3/d	Qw Sm^3/d	Total liq. Sm^3/d	GOR Sm^3/Sm^3	WC (-)
W-3/5	96.9	60.1	1395	380405	113	1508	272.7	0.07
W-3/6	104.5	61.1	1234	404743	120	1354	328.0	0.09
W-3/7	105.1	60.7	1251	417639	110	1361	333.8	0.08
W-3/8	119.3	60.3	1420	521047	100	1520	366.9	0.07
W-4/1	45.6	76.9	677	48030	491	1168	70.9	0.42
W-4/2	46.9	79.0	832	70162	871	1703	84.3	0.51
W-4/3	48.2	78.3	752	64143	796	1548	85.3	0.51
W-4/4	49.4	79.0	963	93926	945	1908	97.5	0.50
W-4/5	71.4	77.6	831	134376	724	1555	161.7	0.47
W-4/6	80.2	75.3	773	145585	363	1136	188.3	0.32
W-4/7	99.0	72.1	961	230492	456	1417	239.8	0.32
W-4/8	118.3	70.1	744	332671	486	1230	447.1	0.40
W-4/9	125.4	68.8	875	405449	927	1802	463.4	0.51
W-4/10	135.0	67.8	706	405061	533	1239	573.7	0.43

Table A - 2 Density of gas and oil phases, superficial gas and liquid velocities, no-slip void fractions of measured separator data at flowline pressure and temperature using PVT models, and void fractions obtained by steady state flow simulator PIPESIM

Well / Test No	WHP bara	WHT °C	ρ_g kg/m^3	ρ_o kg/m^3	u_{sG} m/s	u_{sL} m/s	Void No-slip	Void Pipesim
W-1/1	34.1	68.9	29.1	775.7	1.5	0.9	0.61	0.51
W-1/2	34.1	71.6	29.1	774.7	1.7	1.0	0.62	0.51
W-1/3	34.6	70.7	29.5	774.5	1.6	1.0	0.65	0.53
W-1/4	35.1	71.5	29.9	774.1	1.6	1.0	0.67	0.49
W-1/5	35.9	69.4	30.7	763.5	1.3	1.0	0.56	0.44

Well / Test No	WHP bara	WHT °C	ρ_g kg/m³	ρ_o kg/m³	u_{sG} m/s	u_{sL} m/s	Void No-slip	Void Pipesim
W-1/6	36.5	76.1	31.0	771.2	1.6	1.7	0.48	0.36
W-1/7	37.5	67.5	31.7	774.3	1.0	0.8	0.55	0.40
W-2/1	52.3	83.2	41.0	755.0	2.7	4.8	0.32	0.29
W-2/2	55.5	82.7	47.5	750.7	3.2	4.8	0.36	0.35
W-2/3	63.7	82.1	525	725.0	2.1	4.0	0.31	0.27
W-2/4	82.7	81.4	77.8	725.9	6.2	1.5	0.39	0.30
W-2/5	104.4	77.6	92.0	705.0	0.8	1.9	0.51	0.47
W-2/6	122.0	69.9	113.1	693.3	1.0	1.3	0.54	0.54
W-3/1	68.9	60.8	58.4	746.6	2.5	4.3	0.61	0.41
W-3/2	75.8	60.6	64.9	741.0	2.4	5.3	0.61	0.38
W-3/3	84.1	60.6	72.8	734.4	4.1	1.4	0.60	0.37
W-3/4	89.3	58.6	79.8	725.1	3.5	1.5	0.67	0.47
W-3/5	96.9	60.1	79.8	726.2	2.9	1.5	0.63	0.41
W-3/6	104.5	61.1	95.7	711.0	0.3	1.2	0.65	0.44
W-3/7	105.1	60.7	96.5	710.3	0.5	1.7	0.65	0.44
W-3/8	119.3	60.3	112.3	699.4	0.4	1.6	0.63	0.42
W-4/1	45.6	76.9	37.5	760.7	1.1	1.7	0.45	0.25
W-4/2	46.9	79.0	38.6	758.0	1.6	1.6	0.47	0.32
W-4/3	48.2	78.3	39.7	757.4	1.4	1.9	0.47	0.35
W-4/4	49.4	79.0	40.7	755.6	2.0	1.5	0.52	0.46
W-4/5	71.4	77.6	59.5	738.1	2.7	4.3	0.49	0.35
W-4/6	80.2	75.3	67.7	731.6	5.0	1.4	0.55	0.45
W-4/7	99.0	72.1	86.2	717.4	0.5	1.6	0.48	0.40
W-4/8	118.3	70.1	109.8	695.4	0.3	1.2	0.55	0.45

Well / Test No	WHP bara	WHT °C	ρ_g kg/m³	ρ_o kg/m³	u_{sG} m/s	u_{sL} m/s	Void No-slip	Void Pipesim
W-4/9	125.4	68.8	118.1	690.3	0.4	1.7	0.48	0.40
W-4/10	135.0	67.8	131.0	680.8	0.5	1.9	0.54	0.47

Table A - 3 Gas, liquid, mean and slip velocities from steady state flow simulator PIPESIM

Well / Test No	WHP bara	WHT °C	Gas vel (m/s)	Liq vel (m/s)	Mean Vel (m/s)	Slip Vel (m/s)	Void
W-1/1	34.1	68.9	2.57	1.81	2.17	0.76	0.53
W-1/2	34.1	71.6	2.94	2.05	2.47	0.89	0.53
W-1/3	34.6	70.7	2.89	2.04	2.44	0.85	0.55
W-1/4	35.1	71.5	2.67	1.95	2.27	0.72	0.53
W-1/5	35.9	69.4	2.28	1.76	1.98	0.52	0.47
W-1/6	36.5	76.1	3.13	2.88	2.97	0.25	0.39
W-1/7	37.5	67.5	2.09	1.7	1.85	0.39	0.42
W-2/1	52.3	83.2	7.52	7.52	7.52	0	0.33
W-2/2	55.5	82.7	7.75	7.75	7.75	0	0.37
W-2/3	63.7	82.1	5.82	5.82	5.82	0	0.28
W-2/4	82.7	81.4	7.24	7.24	7.24	0	0.33
W-2/5	104.4	77.6	9.82	7.83	8.78	1.99	0.47
W-2/6	122.0	69.9	4.09	3.38	3.84	0.71	0.54
W-3/1	68.9	60.8	3.83	3.05	3.4	0.78	0.49
W-3/2	75.8	60.6	4.14	3.15	3.6	0.99	0.52
W-3/3	84.1	60.6	4.03	3.27	3.6	0.76	0.37
W-3/4	89.3	58.6	4.16	2.85	3.5	1.31	0.59
W-3/5	96.9	60.1	4.75	3.58	4.12	1.17	0.53

Well / Test No	WHP bara	WHT °C	Gas vel (m/s)	Liq vel (m/s)	Mean Vel (m/s)	Slip Vel (m/s)	Void
W-3/6	104.5	61.1	4.7	3.39	4.02	1.31	0.56
W-3/7	105.1	60.7	4.76	3.42	4.07	1.34	0.56
W-3/8	119.3	60.3	5.05	3.82	4.39	1.23	0.53
W-4/1	45.6	76.9	1.89	1.89	1.89	0	0.32
W-4/2	46.9	79.0	4.73	3.2	3.98	1.53	0.45
W-4/3	48.2	78.3	2.83	2.83	2.83	0	0.35
W-4/4	49.4	79.0	2.54	2.54	2.54	0	0.33
W-4/5	71.4	77.6	3.34	3.32	3.32	0.02	0.37
W-4/6	80.2	75.3	3.06	2.82	2.91	0.24	0.35
W-4/7	99.0	72.1	2.86	2.3	2.53	0.56	0.47
W-4/8	118.3	70.1	4.15	3.48	2.94	0.67	0.45
W-4/9	125.4	68.8	3.93	2.86	3.36	1.07	0.46
W-4/10	135.0	67.8	4.83	3.9	4.31	0.93	0.49

Table A - 4 The grouped test data for the pressure range of 40 bara.

Well Test No	WHP bara	WHT °C	Total liq. m^3/d	Water-cut
W-1/1	34.1	68.9	910	0.51
W-1/2	34.1	71.6	1001	0.50
W-1/3	34.6	70.7	1005	0.54
W-1/4	35.1	71.5	991	0.50
W-1/5	35.9	69.4	947	0.51
W-1/6	36.5	76.1	1688	0.68
W-1/7	37.5	67.5	810	0.49
W-4/1	45.6	76.9	1168	0.42
W-4/2	46.9	79.0	1703	0.51
W-4/3	48.2	78.3	1548	0.51
W-4/4	49.4	79.0	1908	0.50
Average	**39.8**	**73.5**	**1244**	**0.52**

Table A - 5 The grouped test data for the pressure range of 65 bara.

Well Test No	WHP bara	WHT °C	Total liq. m^3/d	Water-cut
W-2/3	63.7	82.1	3977	0.89
W-2/1	52.3	83.2	4778	0.91
W-2/2	55.5	82.7	4804	0.89
W-3/2	75.8	60.6	1389	0.04
W-3/1	68.9	60.8	1442	0.08
W-4/5	71.4	77.6	1555	0.47
Average	**64.6**	**74.5**	**2991**	**0.54**

Table A - 6 The grouped test data for the pressure range of 85 bara.

Well / Test No	WHP bara	WHT °C	Total liq. m^3/d	Water-cut
W-2/4	82.7	81.4	4562	0.86
W-3/4	89.3	58.6	1131	0.01
W-3/3	84.1	60.6	1480	0.05
W-4/6	80.2	75.3	1136	0.32
Average	**84.1**	**69.0**	**2077**	**0.31**

Table A - 7 The grouped test data for the pressure range of 105 bara.

Well / Test No	WHP bara	WHT °C	Total liq. m^3/d	Water-cut
W-2/5	104.4	77.6	3754	0.79
W-3/6	104.5	61.1	1354	0.09
W-3/7	105.1	60.7	1361	0.08
W-3/5	96.9	60.1	1508	0.07
W-4/7	99	72.1	1417	0.32
Average	**102.0**	**66.3**	**1879**	**0.27**

Table A - 8 The grouped test data for the pressure range of 125 bara.

Well / Test No	WHP bara	WHT °C	Total liq. m^3/d	Water-cut
W-2/6	122	69.9	1276	0.78
W-3/8	119.3	60.3	1520	0.07
W-4/8	118.3	70.1	1230	0.40
W-4/9	125.4	68.8	1802	0.51
W-4/10	135	67.8	1239	0.43
Average	**121.3**	**67.3**	**1457**	**0.44**

B. Results From Field Measurements

Table B - 1 Test data and measured pressure wave propagation speed together with their standard deviation for the pressure range of 40 bara.

Well / Test No	WHP bara	WHT °C	Total liq. m^3	Water-cut	Void Fraction	PrsWave Speed m/s	STD m/s	STD-Rel %	G/L Flow Pattern
W-1/1	34.1	68.9	910	0.51	0.61	176.8	24.8	14.0	Slug
W-1/2	34.1	71.6	1001	0.50	0.62	187.7	10.4	5.5	Slug
W-1/3	34.6	70.7	1005	0.54	0.65	189.8	8.8	4.6	Slug
W-1/4	35.1	71.5	991	0.50	0.67	184.9	15.9	8.6	Slug
W-1/5	35.9	69.4	947	0.51	0.56	182.8	19.5	10.7	Slug
W-1/6	36.5	76.1	1688	0.68	0.48	148.4	14.9	10.0	Slug
W-1/7	37.5	67.5	810	0.49	0.55	176.1	5.2	2.9	Slug
W-4/1	45.6	76.9	1168	0.42	0.45	178.9	10.7	6.0	Slug
W-4/2	46.9	79.0	1703	0.51	0.47	166.7	8.7	5.2	Slug
W-4/3	48.2	78.3	1548	0.51	0.47	172.6	8.4	4.9	Slug
W-4/4	49.4	79.0	1908	0.50	0.52	163.8	9.8	6.0	Slug
Average	**39.8**	**73.5**	**1244**	**0.52**	**0.55**	**175.3**	**12.5**	**7.1**	

Table B - 2 Test data and measured pressure wave propagation speed together with their standard deviation for the pressure range of 65 bara.

Well / Test No	WHP bara	WHT °C	Total liq. m^3	Water-cut	Void Fraction	PrsWave Speed m/s	STD m/s	STD-Rel %	G/L Flow Pattern
W-2/3	63.7	82.1	3977	0.89	0.31	191.8	18.9	9.9	Dispersed Bubble.
W-2/1	52.3	83.2	4778	0.91	0.32	198.8	20.3	10.2	Dispersed Bubble.
W-2/2	55.5	82.7	4804	0.89	0.36	136.8	4.1	3.0	Dispersed Bubble.
W-3/2	75.8	60.6	1389	0.04	0.61	156.7	1.8	1.1	Dispersed Bubble.
W-3/1	68.9	60.8	1442	0.08	0.61	156.5	8.0	5.1	Dispersed Bubble.
W-4/5	71.4	77.6	1555	0.47	0.49	154.5	8.4	5.4	Dispersed Bubble.
Average	**64.6**	**74.5**	**2991**	**0.54**	**0.45**	**165.9**	**10.2**	**5.8**	

Table B - 3 Test data and measured pressure wave propagation speed together with their standard deviation for the pressure range of 85 bara.

Well / Test No	WHP bara	WHT °C	Total liq. m^3	Water-cut	Void Fraction	PrsWave Speed m/s	STD m/s	STD-Rel %	G/L Flow Pattern
W-2/4	82.7	81.4	4562	0.86	0.39	203.3	31.8	15.6	Slug
W-3/4	89.3	58.6	1131	0.01	0.67	165.6	1.2	0.7	Slug
W-3/3	84.1	60.6	1480	0.05	0.60	169.0	7.5	4.5	Slug
W-4/6	80.2	75.3	1136	0.32	0.55	166.8	6.6	3.9	Slug
Average	**84.1**	**69.0**	**2077**	**0.31**	**0.55**	**176.2**	**11.8**	**6.2**	

Table B - 4 Test data and measured pressure wave propagation speed together with their standard deviation for the pressure range of 105 bara.

Well / Test No	WHP bara	WHT °C	Total liq. m^3	Water-cut	Void Fraction	PrsWave Speed m/s	STD m/s	STD-Rel %	G/L Flow Pattern
W-2/5	104.4	77.6	3754	0.79	0.51	146.5	48.7	33.2	Elongated Bubble
W-3/6	104.5	61.1	1354	0.09	0.65	196.7	4.9	2.5	Elongated Bubble
W-3/7	105.1	60.7	1361	0.08	0.65	181.4	6.8	3.8	Elongated Bubble
W-3/5	96.9	60.1	1508	0.07	0.63	180.6	6.7	3.7	Slug
W-4/7	99	72.1	1417	0.32	0.48	178.8	9.3	5.2	Elongated Bubble
Average	**102.0**	**66.3**	**1879**	**0.27**	**0.58**	**176.8**	**15.3**	**9.7**	

Table B - 5 Test data and measured pressure wave propagation speed together with their standard deviation for the pressure range of 125 bara.

Well / Test No	WHP bara	WHT °C	Total liq. m^3	Water-cut	Void Fraction	Acc. Vel m/s	STD	STD-Rel %	G/L Flow Pattern
W-2/6	122	69.9	1276	0.78	0.54	250.2	4.0	1.6	Slug
W-3/8	119.3	60.3	1520	0.07	0.63	200.7	3.9	2.0	Elongated Bubble
W-4/8	118.3	70.1	1230	0.40	0.55	166.8	6.6	3.9	Elongated Bubble
W-4/9	125.4	68.8	1802	0.51	0.48	204.4	4.8	2.4	Elongated Bubble
W-4/10	135	67.8	1239	0.43	0.54	222.5	5.6	2.5	Elongated Bubble
Average	**121.3**	**67.3**	**1457**	**0.44**	**0.55**	**205.5**	**4.8**	**2.5**	

CURRICULUM VITAE

Surname, Name: Özdemir, Rabia Tuğçe

EDUCATION

Degree	Institution	Year of Graduation
MS	METU Information Systems	2021
MS	METU Petroleum and Natural Gas Engineering	2015
BS	METU Petroleum and Natural Gas Engineering	2012
High School	Başkent Üniversite Kolej Ayşeabla Fen Lisesi, Ankara	2006

FOREIGN LANGUAGES

Advanced English, Intermediate Russian

PUBLICATIONS

1. Ozdemir, R. T., Durgut, I., & Reed, M. (2019). Random walk particle-tracking method for modeling changes of sediment characteristics in marine sediments after drilling discharges. *Marine Pollution Bulletin*, *145*, 224–238. https://doi.org/10.1016/j.marpolbul.2019.05.039

WORK EXPERIENCE

Degree	Institution	Year of Graduation
Flow Assurance Engineer	TP-OTC – Black Sea Upstream	2021-Present
Research Assistant	METU Petroleum and Natural Gas Engineering	2012-2021